Boundary Layer Structure and Dynamics in Outer Hurricane Rainbands. Part II: Downdraft Modification and Mixed Layer Recovery

MARK D. POWELL

NOAA Hurricane Research Division, AOML Miami, Florida

(Manuscript received 21 March 1989, in final form 9 November 1989)

ABSTRACT

Recent aircraft boundary layer measurements in the vicinity of principal hurricane rainbands have confirmed that convective downdrafts are capable of transporting cool, dry, low equivalent potential temperature (θ_E) air to the surface, where the mixed layer is eliminated. The incorporation of this air into convection near the core of the storm may weaken the storm, depending upon the scale of the disturbance and the processes governing the recovery of the air while it is flowing toward the eyewall. This paper examines the thermodynamic characteristics of the boundary layer in outer convective hurricane rainbands, providing evidence for downdraft modification mechanisms and determining the extent to which disturbed boundary-layer air may be restored on its trajectory to the storm.

1. Introduction

The boundary layer has long been recognized as an energy source for the tropical cyclone. One of the earliest appraisals of the importance of the hurricane planetary boundary layer (HPBL) came from Byers (1944). He hypothesized that to maintain the observed near-isothermal inflow to the storm at low levels, the air must extract large amounts of sensible heat through turbulent fluxes at the sea surface. Thus, any adiabatic cooling is offset as the air flows toward lower pressure. Malkus and Riehl (1960) reasoned that the sea-surface heat and moisture source is required to increase the equivalent potential temperature of inflowing air to values high enough to support the low hydrostatic central surface pressure of the eye. Numerical simulations, such as those by Ooyama (1969), relied on the boundary layer moisture supply to sustain the latent heat release necessary to maintain the warm core storm. Malkus and Riehl developed an empirical relationship between the change in minimum sea-level central pressure of a storm (p_S) and the corresponding change in equivalent potential temperature (θ_E),

$$\delta p_S \approx -2.6\delta\theta_E. \quad (1)$$

Subsequent theoretical developments of this idea by Emanuel (1986) and Betts and Simpson (1987) have reiterated the importance of the surface θ_E supply although with slightly higher values of the proportionality constant.

Although the hurricane surface layer is still believed to be near-isothermal (as well as can be determined from the very limited amount of data available), Frank (1977) and Anthes and Chang (1978) suggest that the sensible heat input from turbulent exchange at the sea surface may not be the dominant mechanism contributing to isothermal inflow. Turbulent entrainment of high potential temperature air from above the boundary layer may also act to supply heat to the inflowing air. Along a constant-temperature inflow trajectory to the core of the storm, an increase of surface θ_E is thought to be produced by enhanced surface moisture flux caused by increasing winds near the storm center, coupled with decreasing surface pressure (which allows a higher saturation specific humidity).

Any mechanisms that can act to lower θ_E, if acting on large enough scales to modify a significant portion of the inflowing boundary layer, should also be able to affect storm intensity. A decrease of θ_E over a portion of the ascent region in the eyewall, for instance, should cause pseudoadiabatic ascent to occur on a cooler moist adiabat such that release of latent heat in the upper and middle troposphere would be decreased. This, together with any related decrease in compensating subsidence in the eye, would result in a cooling of the warm core and a hydrostatic surface pressure increase.

Throughout the paper we will use the terms HPBL and "mixed layer." The mixed layer is defined as the depth over which vertical profiles of the dry static energy (s) and mixing ratio (q) show little variation and are, therefore, "well mixed." The mixed layer is capped by a marked stable and dry layer known as the "transition layer," above which s increases with height and q decreases with height at a moderate rate. Here we

Corresponding author address: Mark D. Powell, NOAA/Environmental Research Laboratories, Hurricane Research Division/AOML, 4301 Rickenbacker Causeway, Miami, FL 33149.

assume that the mixed-layer depth identifies the region over which small-scale, surface-induced turbulence generated mechanically, and/or by buoyancy, occurs continuously in time (Moss 1978). As such, the mixed-layer depth is synonymous with the HPBL height and the two terms are hereafter used interchangeably.

Documentation of boundary layer modification has been obtained through low level measurements made in tropical, non-hurricane convection. Observational studies of tropical squall line systems investigated in the Atlantic Tropical Experiment of the Global Atmospheric Research Program (GATE) (e.g., Johnson and Nicholls 1983; Zipser 1977; Fitzgarrald and Garstang 1981a,b), the Barbados Oceanic and Meteorological Experiment (BOMEX) (e.g., Zipser 1969) and the Venezuelan International Meteorological and Hydrological experiment (VIMHEX) (e.g., Betts 1976) have investigated the role of downdraft interaction with the boundary layer. In the wake of a squall line, cooler, dryer, downdraft-transported air persisted near the surface for several hours. The wake region was characterized by low θ_E magnitudes near the surface and a shallow mixed layer. For such areas to support convection, provided favorable conditions aloft, it is necessary that the boundary layer recover to a well-mixed state with high values of θ_E. Zipser (1977) found a near-constant mixed layer height of 200 m in the wake area, implying that mixed layer growth was suppressed by mesoscale downward motion from unsaturated downdrafts in rain falling from the trailing anvil. Nicholls and Johnson (1984) used a sophisticated mixed layer model to calculate recovery of the wake mixed layer in a GATE squall line. Their comparisons to observed composite fields suggested that mixed layer entrainment was enhanced by rainfall evaporation. Based on the aforementioned studies, modification of the boundary layer takes place on very large spatial scales (thousands of square kilometers), and restoration requires several hours for recovery to pre-squall conditions.

Measurements of boundary layer modification for hurricanes are more difficult than in squall lines since cold downdraft outflows may be too shallow to be safely sampled by research aircraft. Low-level aircraft observations in Hurricane Gladys (1975) as described by Peter Black (personal communication, 1988) and Hurricane Floyd (1981) by Barnes et al. 1983, have indicated the presence of low θ_E air at the 150 m level, adjacent to rainband convection. Barnes et al. 1983 (hereafter referred to as BZJM) determined that the air was transported from middle levels of the rainband in downdrafts.

In addition, recent modeling investigations by Rosenthal (1978), Lord et al. (1984), Rotunno and Emanuel (1987) and Yamasaki (1986) have identified mechanisms with the potential of modifying the HPBL (although without resolution of the convective scales). The key mechanisms they emphasized were the importance of mesoscale downdrafts and their interaction with boundary layer inflow. Modeling efforts by Anthes and Chang (1978) and observational programs described by Black (1983) have pointed out the potential for the boundary layer air to be modified through contact with cold sea surface temperatures in the wake of mature tropical cyclones. These features, if found to be common features in hurricanes, and depending on their scale, may prove to be mechanisms capable of limiting storm intensity below the potential (Merrill 1987; Emanuel 1988) deduced from evaluating sea surface and outflow temperatures.

In Part I, the rainfall and kinematic structures of the hurricane planetary boundary layer (HPBL) in the vicinity of outer rainbands in Hurricanes Josephine and Earl were examined. This paper will build on that effort by investigating the influence of the rainband on the mesoscale thermodynamic structure of the HPBL. The emphasis will be on the effect of downdrafts as a mechanism for altering boundary layer heat and moisture structure. Based upon analyses of Hurricanes Josephine (1984) and Earl (1986) and comparisons to the Hurricane Floyd (1981) study by Barnes et al. (1983), this paper contends that regions of downdraft-modified HPBL are indeed a common feature of convectively active hurricane rainbands. These regions have a preference for the upshear side of the rainband axis and may occupy several thousand square kilometers with disturbed air in various stages of recovery. A mixed layer model is used to show the conditions governing the recovery of this air, including those in which the restoration of modified air may not be completed before the air reaches the eyewall of the storm. Incomplete restoration of disturbed air may be responsible for weakening the hurricane through cooling the core of the storm, with a subsequent rise in the central pressure.

2. Thermodynamic measurements

Details on the NOAA aircraft instrumentation characteristics are available in Merceret and Davis (1981). Aircraft thermodynamic measurements are prone to errors caused by high liquid water content in clouds and rain (e.g., LeMone 1980). The procedure followed to correct sensor wetting problems is the same as that followed by Barnes et al. (1983) and Barnes and Stossmeister (1986).

Thermodynamic sounding information in Hurricane Earl was supplemented by Omega Dropwindsondes (ODWs) dropped from both aircraft in Hurricane Earl. The use of ODWs in hurricane research (Burpee et al. 1984; Franklin et al. 1988) is especially helpful in the HPBL where aircraft profiles are time consuming and difficult to perform. Since ODWs continues to be used for determining the thermodynamic and flow fields surrounding hurricanes (and other moist nontropical environments), it is important that their

shortcomings be realized. Although it is difficult to determine errors by comparison with aircraft soundings without sampling the same air volumes, it was apparent that the ODW humidity measurements suffered sensor wetting or a lack of sensitivity in high humidity conditions. Correction of the data for sensor-wetting errors was limited to the subcloud layer and consisted of substituting a constant q lapse rate wherever the temperature profile was dry adiabatic. No correction was made above 500 m; hence the q and TD profiles to be shown from the ODWs are biased, especially above the mixed layer. We present the ODW q profiles for comparison to aircraft profile shapes, but rely upon the aircraft humidity data for contrasting the outer and inner sides of the rainband.

A comparison of five ODW and aircraft profiles in close proximity on the outer side of the Earl rainband (see Powell 1988, for details) indicated that, in general, ODW dewpoints measured in the high humidity conditions of the lower levels are 1–1.5°C higher than the corresponding aircraft measured dewpoints from 80 to 500 m altitudes. ODW temperatures appear to be about 1°C cooler than the aircraft, but are well within the range of aircraft values. Although ODW temperature measurements are of reasonable quality, the humidity problem is serious and warrants redesign of the sensor. A new humidity sensor design featuring a heated hygristor is under consideration at the National Center for Atmospheric Research (NCAR) (James Franklin 1988, personal communication) for possible use by 1990.

3. Mesoscale thermodynamic structure in outer rainbands

In Part I, the wind and precipitation fields showed a strong two-dimensional mesoscale structure superimposed with three-dimensional convective scale features leading to a schematic conceptual model for the quasi-stationary outer convective rainband. In this section we follow the same approach to present the two-dimensional mesoscale fields of thermodynamic quantities relative to the rainband axis of Earl. Although less thermodynamic data were available in Hurricane Josephine, its structure will also be discussed for comparison. Numerous aircraft and ODW soundings of dry static energy ($s = C_pT + gZ$, where C_p is specific heat, T is temperature, g is the gravitational constant, and Z is height), and specific humidity adjacent to the rainbands are also presented. With these soundings, we show that the inner and outer sides of the Earl (and to some extent Josephine) principal rainband are distinctly different.

Flight-level thermodynamic measurements were composited relative to the band according to the method described in Part I. Sea-surface temperatures in the vicinity of the Earl rainband were 27°C and surface pressures were ~1015 mb, yielding saturation surface values of potential temperature (θ), θ_E, s and q of 298.9 K, 365.3 K, 301.5 J g^{-1} and 22 g kg^{-1} respectively. The Simpson (1978) method was used to calculate θ_E. The reader may wish to refer to the corresponding reflectivity and kinematic analyses described in Part I.

a. *Crossband profiles*

Crossband–height sections made from profiles in the northern portion of the rainband are presented in Figs. 1a–d. The θ profile (Fig. 1a) shows a decrease at the band axis and higher θ values on the outer side of the band at low levels. The specific humidity field (Fig. 1b) shows a double maximum associated with the Y-shaped precipitation element at 1350 m. Larger values near the axis and 2 g kg^{-1} higher values on the outer side (19.5 g kg^{-1}) are shown at 150 m. The θ_E cross section in Fig. 1c has double maxima of 350 K at 1350 m similar to those in q. At 150 m higher values are found near the axis with values on the outer side of the band of 359 K, almost 10 K higher than those on the inner side of the band. The relative humidity (RH) in Fig. 1d shows near-saturation, except below 1350 m where RH drops below 90% over 12 km from the axis.

By comparing these analyses with the kinematic analyses in Part I, we find that the cooler and drier air at low levels is associated with a downdraft spreading out near the surface on the inner side of the band axis. This is the downdraft region identified in Part I (Fig. 13e). The θ_E values at 150 m on the inner side of the band are of the same order as θ_E values at 1350 m. This suggests that downdraft air (conserving the low θ_E from above) spreads out and mixes with the air at 150 m. This aspect of modification of the HPBL will be discussed in more detail in the next section.

Thermodynamic cross sections at the southern portion of the Earl band also show slightly higher values of θ and q on the outer side of the rainband axis. These cross sections (not shown) showed only transient evidence of HPBL modification by downdrafts on the inner side of the band. The failure to find significant long-lived modification may have been caused, in part, by difficulties in positioning the aircraft for optimal transit of a particular rainfall element. Subsequent alongband and crossband flight-level data collected during a Doppler radar pattern at 1500 m indicates thermodynamic structure similar to that discussed above, except for areas of mesoscale descent below the stratiform anvil rain area on the outer side of the rainband. These areas are ~20 km (alongband scale) and are characterized by very dry air of 70% RH, dewpoint depressions of 4°C, q of 10–11 g kg^{-1}, θ_E values of 336–338 K and downward motion of 0.1–0.5 m s^{-1}.

Crossband profiles (not shown) in the Hurricane Josephine rainband were conducted at the 500 and 1500 m levels. Although not as dramatic as in Hurri-

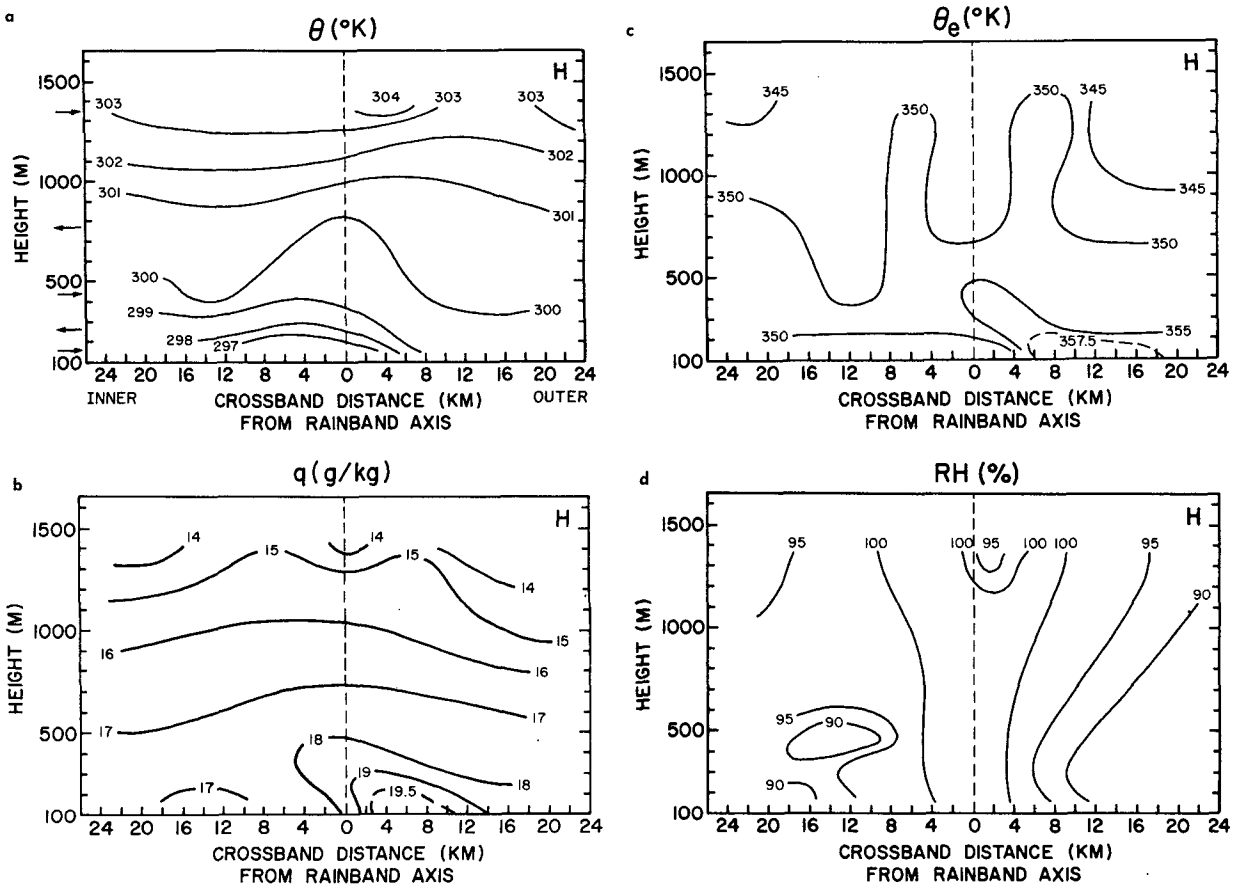

FIG. 1. Analyses from crossband flight profiles in Hurricane Earl of (a) potential temperature (θ), (b) specific humidity (q), (c) equivalent potential temperature (θ_E), (d) relative Humidity (RH). Dashed vertical line refers to 25 dBZ reflectivity axis of rainband.

cane Earl, slightly higher θ, larger dewpoint depressions, lower q, and lower θ_E were found on the inner side of the rainband associated with downward motion in a region of positive divergence (Part I; Figs. 10e, f). This dry region may have been a result of subsidence warming during descent. The more moist air on the outer side of the band might have been prevented from reaching the inner side by the rainband barrier (zero inflow line, Part I; Figs. 9d, 10d).

b. Detailed HPBL structure on the outer side of the rainband

As depicted in Fig. 2, stepped-descent, fixed-bank climb, and ODW soundings were made adjacent to the Earl rainband throughout the experiment. Positions of ODWs indicate where each was launched (from 850 mb). Wind drift of the ODWs would cause their final position to be 6–8 km downstream. Additional details on the soundings are listed in Table 1. A total of 11 soundings were made on the outer side of the band from 1644 to 1750 UTC, covering an alongband distance of ~120 km.

As shown in Part I for the precipitation and kinematic structure, certain aspects of the thermodynamic structure on the outer side of the Earl rainband have much in common with that of Hurricane Floyd (BZJM) and tropical squall lines. Therefore, it is reasonable to expect that similar processes govern the mixed-layer structure of both hurricane and tropical rainbands. Representative Skew T–log P diagrams for soundings on the outer side of the rainband in Fig. 3 depict a relatively warm, moist (higher q) mixed layer defined by a dry adiabatic lapse rate to 950 mb, where it is capped by one or more stable layers, including a layer with large dew point depressions of ≥ 6°C (RH of ~65%) from 960–860 mb. On some soundings (Fig. 3b), this large dewpoint depression layer is capped by a moist layer such that the area between T and TD on a skew T plot has a "diamond" shape.

The dry layer between 960 and 860 mb (Fig. 3), is similar to the outer profile in Hurricane Floyd (BZJM) which exhibited dewpoint depressions of 5–6 K amidst mesoscale descent of about 0.5 m s^{-1} at the 850 mb (1500 m) level. The positions of the Earl and Floyd bands on the front right and front sides of the storm

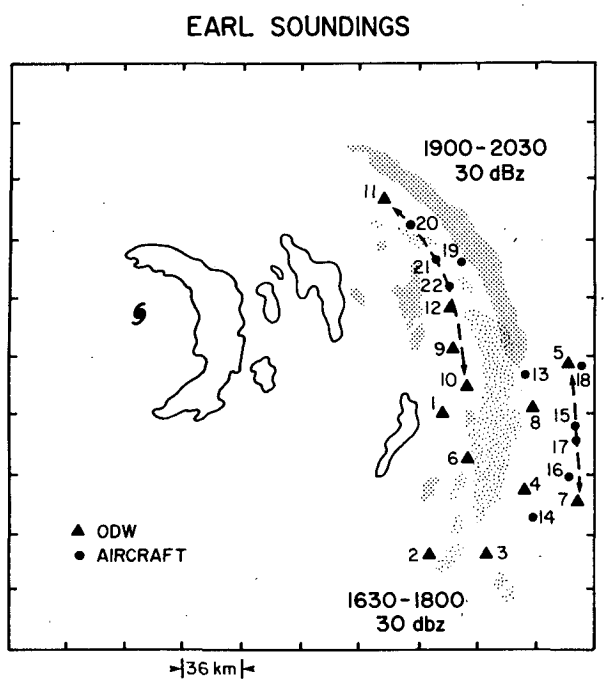

FIG. 2. Locations of Earl aircraft and ODW soundings with respect to the rainband, showing schematic 30 dBZ LF radar reflectivity contours for two time periods. Numbers refer to soundings in Table 1. Irregular stipling is associated with main reflectivity features from 1630 to 1800 UTC, regular stipling represents band features from 1900 to 2030 UTC, solid contours represent typical eyewall and secondary band features throughout the experiment.

ensured that the outer side inflow was unaffected by significant convection on its way to the band. A study of Hurricane Irene (1981) by Barnes and Stossmeister (1986) suggests that principal rainbands in the right rear quadrant may show quite different profiles on the outer side of the band, with a more well-mixed profile and absence of a θ_E minimum at middle levels.

Zipser's (1977) collection of soundings depicting a wake region beneath a mesoscale anvil to the rear of a tropical squall line were characterized by a diamond shaped profile. There, the mixed layer was recovering after having been modified by the transport of low θ_E air in near-saturated convective-scale downdrafts within the squall line. Zipser (1969, 1977) suggested that above this modified layer, mesoscale unsaturated downdrafts could transport additional midtropospheric air to lower levels just above the mixed layer and exert a restraining influence on the recovery of the boundary layer. Numerical studies by Brown (1979) and Leary (1980) associate such downdrafts with evaporative cooling of precipitation falling from the anvil of the system.

The Earl rainband anvil is limited in crossband extent to within 15–20 km of the band axis. Sounding 13 (Fig. 3a) was taken beneath the rainband anvil and was associated with rainfall evaporation (the aircraft passed through rain at 930 mb). Soundings 7 and 17 (Figs. 3a,b) were taken, under the higher (base, ~7 km), thinner, vortex-scale anvil about 30 km outward from the rainband and are associated with mesoscale subsidence.

In comparing the above soundings of Hurricanes Earl (Fig. 3) and Floyd (BZJM) with the Zipser soundings, the crucial difference lies in the character of the air within the mixed layer. The lower levels in the squall-line wake cases were near saturation and relatively cool, a consequence of boundary-layer modification by downdrafts within the squall line convection. Analyses of tropical squall-line wind fields (e.g., Gamache and Houze 1982) show the wake area as the outflow side. The HPBL soundings on the outer side

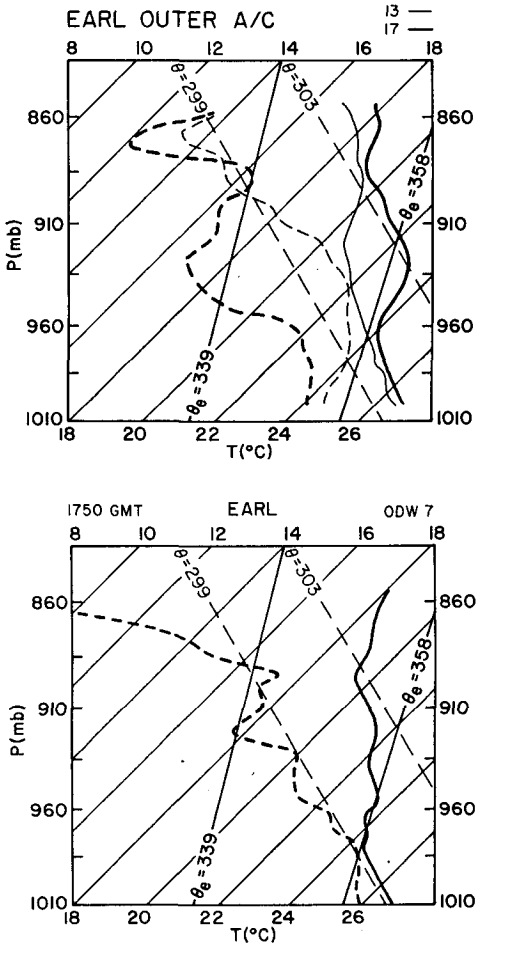

FIG. 3. Skew T–log P diagrams for profiles on the outer side of the Earl rainband. (a) Aircraft soundings: 13 (Temperature (T) is thin solid line, dewpoint temperature (TD) is thin dashed line), 17 (T is thick solid line, TD is thick dashed line). (b) ODW sounding 7. Dashed lines sloping right to left are dry adiabats labeled by potential temperature values of 299 and 303 K, steep sloping solid lines are pseudoadiabats labeled by equivalent potential temperature values of 358 and 339 K, gentler sloped lines from left to right are isotherms labeled in Celsius.

of the Earl rainband had relatively warm, and moist (higher q) mixed layers. As discussed in Part I, the outer side of the Earl rainband was the inflow side. In the hurricane, on the inflow side of the rainband, the depth of the boundary layer is modulated by the strength of the mesoscale descent and precipitation evaporation below the rainband-scale and storm-scale anvil regions.

c. *Detailed structure on the inner side of the rainband*

As shown in Fig. 2, the 11 thermodynamic profiles taken on the inner side of the rainband cover an along-band distance of 180 km from 1638 to 1946 UTC. Representative skew T–log P diagrams for the inner soundings are shown in Fig. 4. The aircraft profiles in Fig. 4a show a contrast between a strongly modified cooler, drier, HPBL (profile 20), and a warmer (but still cooler than the outer side), more moist HPBL in the vicinity of a stratiform secondary band (profile 22). The ODW soundings in Figs. 4b,c are uncorrected for sensor wetting and, therefore, show saturated conditions. They show varying mixed-layer and transition-layer depths with profile 1 (Fig. 4b) showing a very shallow mixed layer of 200 m slightly upband of the region of low θ_E found at 1715 during the crossband profiles. Profile 2 (Fig. 4c) was made at the same time as profile 1, but about 70 km upband where the band's convection was weaker. It shows a deeper (375 m), warmer, mixed layer.

The thermodynamic structure of the inner side of the Earl rainband exhibits a diverse range, from near absence of a mixed layer (due to replacement by cool, dry air) to various stages of recovery of the layer by surface heat and moisture fluxes and turbulent mixing and entrainment processes, to a mixed layer similar to, but moister than, the inflow side of the rainband. As suggested by BZJM, the cool, dry air at the lower levels probably has its origins in the midlevel inflow of low θ_E air that is transported to the surface by convective-scale downdrafts on the inner side of the rainband axis. Not all the air on the inner side of the band is modified however, some of the air flows around cells and between breaks in the band to arrive at the inner side with an undisturbed mixed layer structure as suggested by ODW profile 2 (Fig. 4c).

d. *Characteristic mixed-layer structures*

Profiles of s and q from the outer and inner sides of the Earl rainband in Figs. 5 and 6 reflect the characteristic mixed layer structures. The outer side profiles are similar to the undisturbed or presquall profiles of the tropics (e.g., Betts 1976; Zipser 1977; Fitzgarrald and Garstang 1981a). Both aircraft and ODW profiles of dry static energy (Fig. 5a,b) on the outer side of the band display a mixed-layer structure from the surface to 500–600 m (labeled **h** on sounding 11, Fig. 5b) followed by a transition layer (labeled Δ**h** on sounding 11) in which s increases sharply before resuming a more gentle increase with height (Γ_S in sounding 11). A tab-

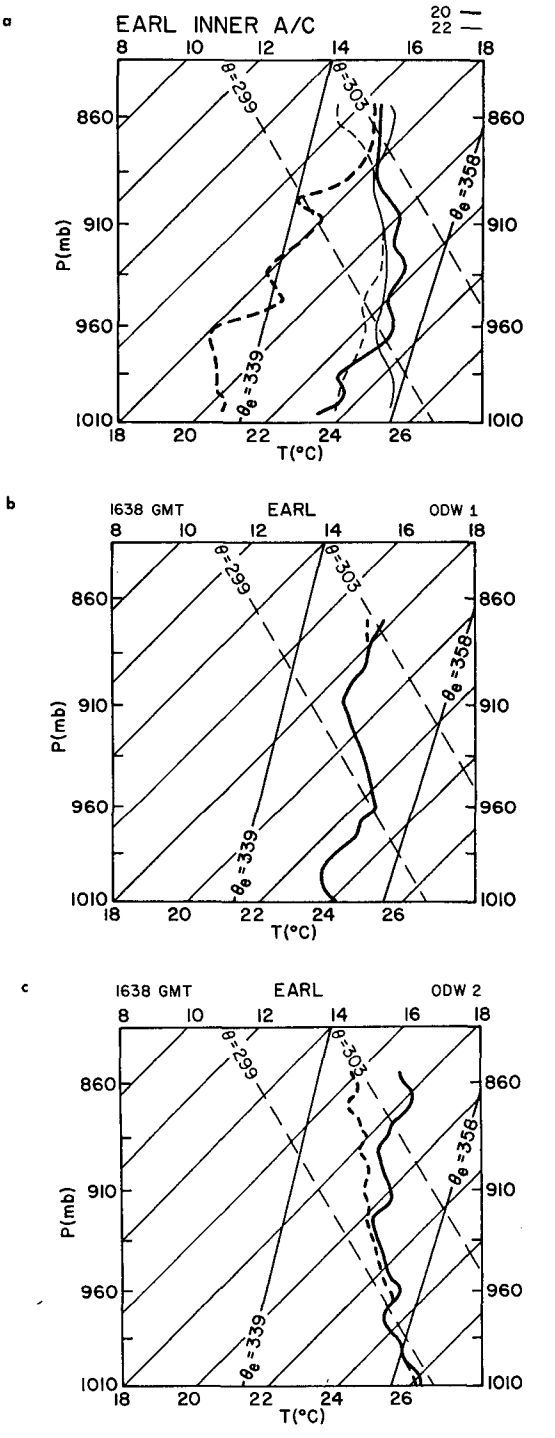

FIG. 4. As in Fig. 3 but for the inner side of the Earl rainband. (a) Aircraft sounding 20 (Temperature is thick solid line, dewpoint temperature is the thick dashed line) and sounding 22 (temperature is the thin solid line, dewpoint is thin dashed line), (b) ODW sounding 1, (c) ODW sounding 2.

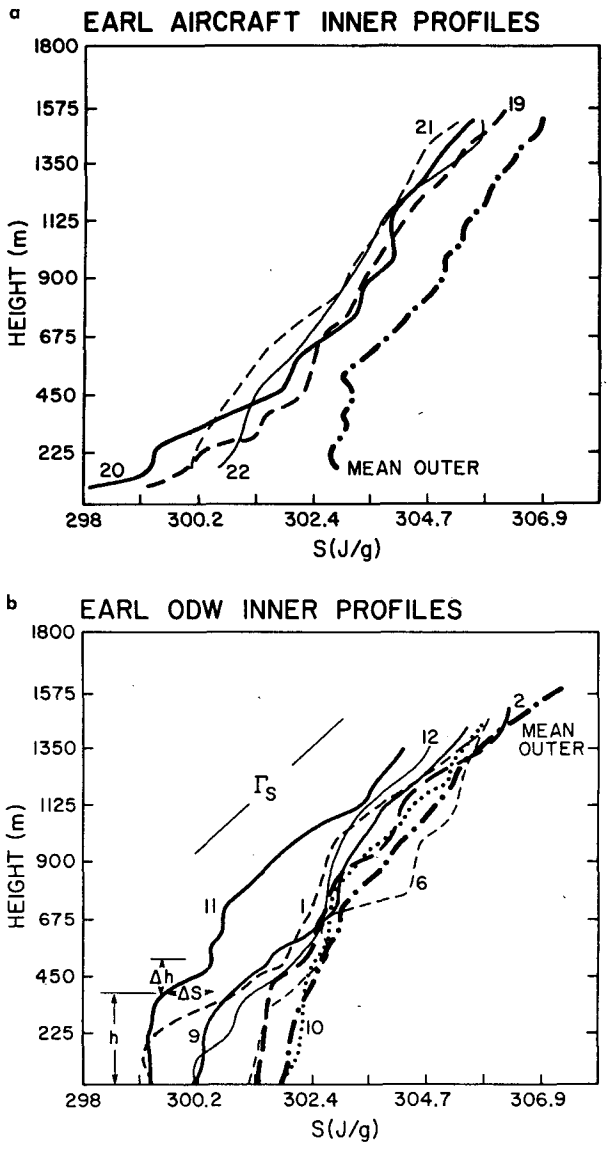

FIG. 5. Dry static energy (S) profiles adjacent to the Hurricane Earl outer rainband. (a) Aircraft profiles 19–22 conducted on the inner side of the rainband from 1916 to 2000 UTC and mean of all outer side aircraft profiles, executed from 1721 to 1803 UTC, (b) ODW profiles on the inner side of the rainband and mean of all ODW profiles from the outer side of the rainband. Mixed-layer depth (h), transition layer thickness (Δh), lapse rate of dry static energy (Γ_s) and jump in dry static energy over the transition layer (Δs) are indicated for sounding 11.

ulation of mixed layer depths and transition layer thicknesses for all the aircraft and ODW soundings is included in Table 1. The mixed and transition layers were not always well-defined however, hence the missing values in Table 1.

The s profiles on the inner side of the rainband show a distinctly different range of shapes from those that are on the outer side of the rainband. The four aircraft soundings (Fig. 5a) show evidence of a disturbed boundary layer with s values 2–4 J g^{-1} cooler than those on the outer side of the band. The two most disturbed soundings, (profile 20 and the lower part of aircraft stepped-descent profile 19) occurred in proximity to each other at approximately 1930 UTC and show a very shallow or nonexistent mixed-layer structure. The range of ODW profiles in Fig. 5b indicates mixed layers in varying stages of modification, including three (profiles 10, 11, and 12) near the location of the s modification at 1930 UTC, and one (profile 1) near the location of the low θ_E air observed during the crossband profile (Fig. 1c).

Aircraft and ODW mixing ratios (Fig. 6a,b) decrease

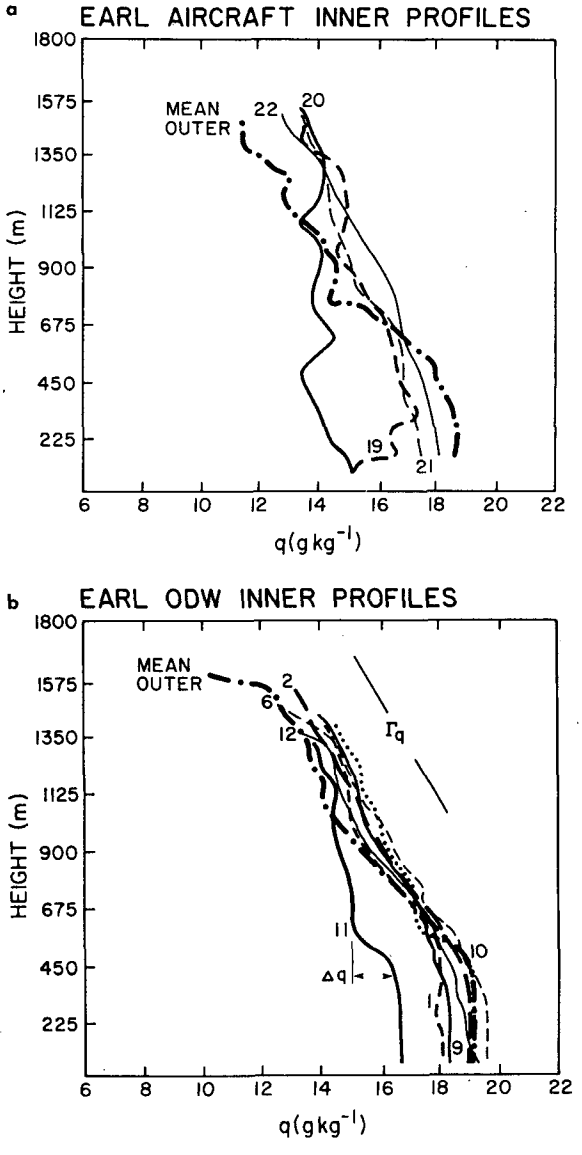

FIG. 6. As in Figs. 5a and 5b but for specific humidity. Lapse rate of specific humidity (Γ_q) above the transition layer and jump in specific humidity across the transition layer (Δ_q) in Fig. 5b are mixed-layer model parameters that are shown for sounding 11.

TABLE 1. Earl thermodynamic soundings.

Sounding	Aircraft*	Time (UTC)	Position with respect to rainband	Mixed layer depth (m)	Transition layer thickness (m)	Surface θ_E (K)
			Omega Dropwindsondes (ODW)			
1	H	1638	Inner, North	200	290	348.3
2	I	1638	Inner, South	375	160	353.4
3	I	1644	Outer, South	540	225[a]	355.0
4	I	1729	Outer, South	495	135[a]	355.9
5	H	1730	Outer, North	530	230[a]	353.0
6	I	1738	Inner, South	315	200	355.3
7	H	1750	Outer, South	360	210	357.4
8	I	1754	Outer, Mid	—[b]	—[c]	—
9	I	1810	Inner, North	315	180[a]	350.7
10	I	1916	Inner, North	420	110	356.0
11	I	1931	Inner, North	340	100	345.0
12	I	1946	Inner, North	135	75	352.8

		Time period (UTC)	Position	Mixed layer depth (m)	Transition layer thickness (m)	LCL (m)	Surface θ_E (m)
			Aircraft soundings				
13	H	1721–1726	Outer, North	500	180[a]	425	357.1
14	I	1725–1729	Outer, South	540	100	468	354.9
15	H	1730–1744	Outer, Mid	530	200	452	355.9
16	H	1744–1750	Outer, South	450	180[a]	486	354.7
17	H	1750–1801	Outer, Mid	520	135	441	355.7
18	H	1801–1803	Outer, North	—[b]	—[c]	425	355.6
19	I	1916–1927	Inner, North	—[b]	—[c]	315	339.6
20	I	1927–1931	Inner, North	—[b]	—[c]	371	340.3
21	I	1932–1944	Inner, North	225	—[c]	353	348.9
22	I	1944–1947	Inner, North	—[b]	—[c]	353	351.2

[a] Transition layer poorly defined.
[b] Undefined mixed layer.
[c] Undefined transition layer.
* I = 43RF; H = 42RF.

gently with height from 18.5 g kg^{-1} at the surface to 450 m, decrease more sharply over a transition layer up to 200 m thick and then lapse at a more gentle rate (Γ_q in sounding 11, Fig. 6b) to as low as 7 g kg^{-1} at 1500 m. The aircraft q profiles on the inner side of the band (Fig. 6a) indicate disturbed conditions, with drying of 1–3 g kg^{-1} below 500 m, and moistening of 1–2 g kg^{-1} relative to the outer aircraft profiles above 1 km. Humidity measurement problems with the ODWs are especially severe on the inner side of the rainband in Fig. 6b. Only profiles 1, 9, and 11 show signs of drier mixed layers than the outer side of the rainband. This mixed layer is not topped by the sharp transition layer with a negative jump in q (Δq in Fig. 6b) that is characteristic of the GATE soundings, however. Only ODW soundings 11 and 10 (Fig. 6b) show signs of a transition layer, and only sounding 11 represents a disturbed profile. The aircraft soundings on the inner side of the band show a positive Δq for the transition layer in sounding 19 and poorly defined transition layers for soundings 20–22. In comparison with the q profiles on the outer side of the band, the inner side profiles are more moist above 500 m and drier below 500 m.

Profiles of s and q in the Hurricane Josephine outer rainband are presented in Fig. 7. The inner side s profiles (Fig. 7a) show an increase with height similar to that shown in Earl. For Hurricane Josephine, the s profile indicates shallow mixed-layer depths of <150–230 m (the lowest altitudes attained in the soundings) for stepped descents SD1 and SD2. The mixed-layer depth on the outer side would have to be <500 m according to sounding 1.

The q profiles in Fig. 7b indicate a slight decrease in q with height up to 600 m, above which a more rapid decrease occurs. Higher q values are found on the outer side of the band which resulted in estimated surface θ_E values of 349 K compared to 345 K on the inner side. In this case however, the θ_E values for the surface air are 5 K warmer than the values at 1500 m. Hence,

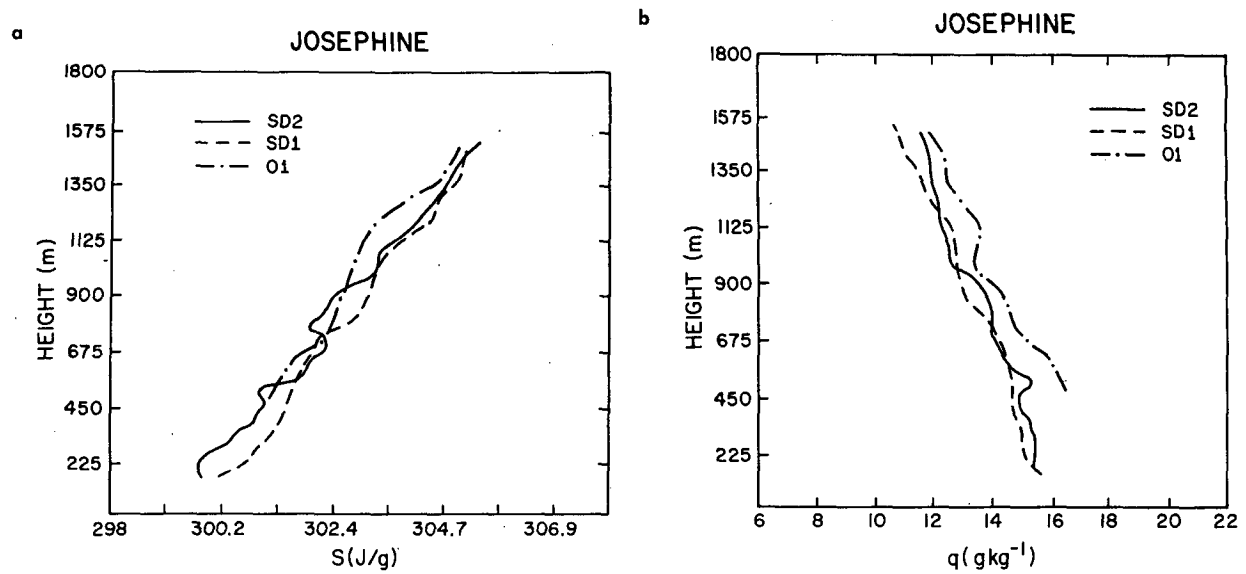

FIG. 7. Profiles executed in an outer convective rainband of Hurricane Josephine from 1100 to 1215 UTC 14 September 1984. SD1 and SD2 are stepped-descent profiles executed on the inner side and 1 is a climb performed on the outer side of the band. (a) Dry static energy (S), (b) specific humidity (q).

there is no evidence of downdraft transport of low θ_E air from middle levels. For Josephine, stable conditions were caused by HPBL modification due to cold sea surface temperatures (see Black et al. 1988, for details).

Despite sea-surface temperatures that are cooler than the air, the saturation specific humidity values at the surface are greater than those in the air, promoting a positive turbulent flux of water vapor from the surface. The near constant or slight decrease in q with height up to 600 m while s increases rapidly suggests that different processes may be involved in the boundary-layer transport of dry static energy and specific humidity in these stable conditions. Usually sea-surface temperatures in hurricanes are high enough to produce unstable or neutral stability conditions with concurrent mixed layers of q and s. In the case of the Josephine HPBL, buoyant eddies may be produced by humidity fluctuations, which can promote upward transport of water vapor from the sea surface. The lack of a surface sensible heat source may prevent the s profile from matching the q mixed-layer height.

e. *Mesoscale mixed-layer variability*

For the Hurricane Earl outer rainband, the combined effects of the processes discussed above produce a mixed-layer structure that is distinctly different from the outer side of the rainband, as illustrated in Figs. 8a,b. Analyses of mixed-layer depth and surface equivalent potential temperature were constructed from the aircraft crossband profiles and the aircraft and ODW soundings listed in Table 1 for two time periods. The first (Fig. 8a) is representative of the rainband during the time period of the crossband profiles while the band was moving outward and the second (Fig. 8b) shows details from the inner side of the band about 2 h later. Mixed-layer depths are significantly more shallow on the inner side of the band, having a mean depth of 240 m compared with 496 m on the outer side of the band.

Surface θ_E values in Fig. 8 were estimated by extrapolation of constant q and θ from the lowest sounding level. Mean surface θ_E on the inner side is 349.2 K compared with 355.5 K on the outer side. Aircraft soundings on the inner side of the band (due to lower surface dewpoint depressions) have lower Lifting Condensation Levels (LCLs in Table 1) than the outer side. The scale of the modification of the boundary layer by the rainband can be estimated in Fig. 8b as being about the length of the convectively active portion of the rainband (150 km) and at least the width of the "moat" region between bands (35 km). In general, this entire area is affected to varying degrees by lower θ_E air near the surface.

The mesoscale crossband analyses of θ_E in Fig. 1c and the θ_E structure suggested by the s and q profiles of Figs. 5 and 6 are very similar to analyses of Floyd presented by BZJM. Their composite crossband profile of θ_E shows minimum values of 342 K on the inner side of the band at 150 m for a decrease of 12 K from the outer side (354 K), while their inner vertical profile has almost constant θ_E with height from 1–6 km in a region of weak mesoscale descent. In both Earl and Floyd, the proximity of stratiform precipitation from secondary bands on the inner side of the primary rainband, together with rain from the rainband's inner anvil, makes for a relatively moist environment compared with the outer side of the band, despite evidence of mesoscale descent.

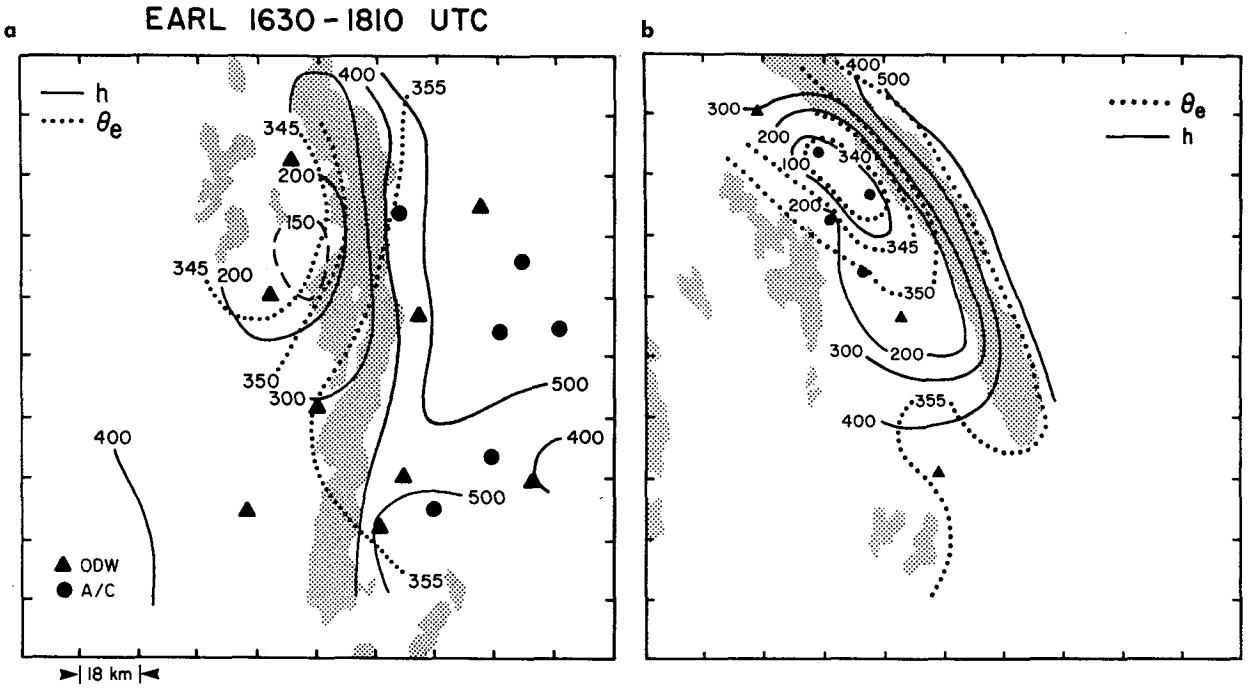

FIG. 8. Analysis of mixed layer heights (solid lines) and equivalent potential temperatures (dotted lines) for soundings adjacent to the rainband. (a) For 180 × 180 km area with schematic band (30 dBZ LF radar contour) from 1630 to 1810 UTC, (b) same as (a) but for 1906–1955 UTC.

In Hurricane Josephine, despite intense reflectivity cells with strong updrafts and downdrafts typical of well-organized convection, no low-level evidence was found for the downdraft transport of low θ_E air characteristic of midlevels. The lack of deep soundings on the outer side of the band prevented documentation of the vertical distribution of θ_E in the middle (600 mb) levels. Sampling of the lowest levels on the inner side (150 m) was made in two locations, but stable conditions might have limited the spreading out of any cool, dry downdraft air to below this level. Hurricane Irene (Barnes and Stossmeister 1986), with weaker inflow, weak low-level convergence and a well-mixed θ_E profile on the outer side, also showed no signs of modification of the mixed layer.

4. Downdraft modification of the HPBL in Hurricane Earl

As mentioned by BZJM, the only possible source for low θ_E of the observed magnitudes is the dry middle-level air generally found at or above 1500 m on the outer side of the band. They found that the more intense reflectivity cells within the Floyd band were associated with a greater number of drafts and downdraft cores. BZJM hypothesized that the low θ_E air on the inner side of the band was transported by convective-scale downdrafts within the band. In this section, we discuss analyses that document three specific examples of HPBL modification by downdrafts in Hurricane Earl.

a. Wake formation behind a moving rainband

The lower three crossband profile flight legs across the northern portion of the band (discussed in Part I and above in section 3a) are presented in time series of 1 s flight-level observations of θ, q, vertical motion (w) and θ_E at the 450 m, 260 m, and 150 m levels in Figs. 9a–c. The reader is referred to the detailed horizontal and VI reflectivity distributions and flight tracks for the legs presented in Part I, Figs. 12c–f. At the 450 m level from 1701–1708 UTC (Fig. 9a), there are three updraft–downdraft couplets on the inner side of the rainband axis near the 25 dBZ reflectivity edge of the band. The updrafts are on a 2–3 km scale while the downdrafts are <1 km in crossband width. Each downdraft is saturated and associated with a minimum in θ, q, and θ_E (after a lag caused by the slow response of the dewpoint sensor). In addition, apart from the individual downdrafts, there is a distinct decrease in θ_E (6 K) and q (2 g kg^{-1}) on the inner side of the rainband.

In the 260 m level pass from 1708–1714 UTC (Fig. 9b), unsaturated downward motion predominates on the inner side of the axis with only one 1 km-scale

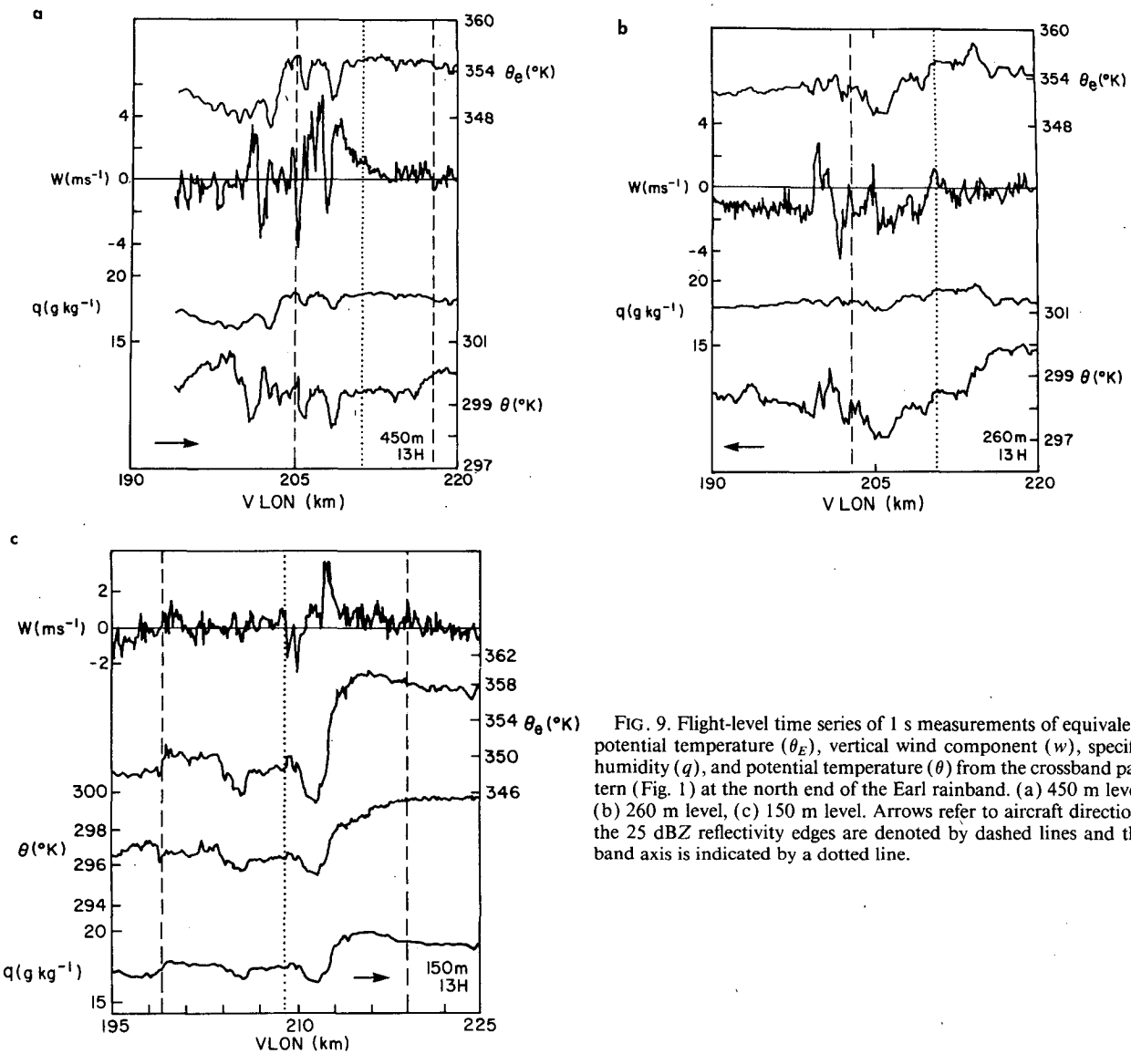

FIG. 9. Flight-level time series of 1 s measurements of equivalent potential temperature (θ_E), vertical wind component (w), specific humidity (q), and potential temperature (θ) from the crossband pattern (Fig. 1) at the north end of the Earl rainband. (a) 450 m level, (b) 260 m level, (c) 150 m level. Arrows refer to aircraft direction, the 25 dBZ reflectivity edges are denoted by dashed lines and the band axis is indicated by a dotted line.

updraft at 8 km from the axis. Here, a large decrease in θ on the inner side of the band axis is correlated with the downward motion and a slight decrease in q, producing lower θ_E values on the inner side.

The pass at 150 m from 1715–1721 UTC (Fig. 9c), shows an updraft–downdraft couplet just outside the band axis. Amidst the increased frequency of the turbulence-induced vertical motion, the 2 km-scale updraft and 0.5 km-scale downdraft demarcate a mesoscale discontinuity in the thermodynamic fields, the downdraft being associated with a convective-scale minimum in θ, q, and θ_E. The collocation of the updraft with the thermodynamic discontinuity demonstrates the partial barrier effect of the rainband updraft. Apart from these minima, however, there is a profound difference in θ, q and θ_E on each side of the band, with θ_E values as low as 345 K on the inner side compared with 358 K on the outer side of the axis.

The $\geqslant$20 km crossband scale of low θ_E air on the inner side of the rainband cannot be attributed to one downdraft. The increased smaller scale turbulence indicates that the downdrafts that had been evident on the earlier passes are already spreading out and detraining upon reaching the 150 m level. The lack of continuity in the w profiles from pass to pass indicates that, instead of one or two particular convective-scale, saturated, downdrafts descending and spreading out at lower levels, there is an accumulation of cooler, lower q air from several downdrafts collecting near the surface on the inner side of the band, as a wake, while the rainband continues moving to the east (as shown by the band edge virtual longitude versus time plot in Fig.

5 of the Part I paper). The cumulative effect of these downdrafts on the inner side of the rainband axis produces mesoscale minima in the thermodynamic fields and a maximum in the crossband divergence near the surface. Despite the obvious presence of turbulence produced mechanically through wind shear, a composite sounding for the inner side of the band from the northern crossband analyses (not shown) indicates that the layer from 150–450 m is very stable and devoid of any mixed-layer structure.

The crossband-scale of this stable lower layer is at least 20 km (the same scale as the similar feature observed by BZJM in Hurricane Floyd's storm-stationary rainband), but little is known of its alongband scale and time scale. Upon discussion of these observations with Gary Barnes of NCAR (personal communication, February 1988), he reexamined the 1 s data collected in Floyd and noted similar correlations of low θ_E air with downdrafts above the 150 m level. Hence, the process responsible for the transport of low θ_E air from middle levels to the boundary layer does, indeed, appear to be convective-scale downdrafts, as hypothesized by BZJM. Outward motion of a rainband, such as in Earl, could produce a relatively large scale wake (depending on the storm-relative outward motion of the band) similar to that produced by tropical squall lines.

b. Downdraft spreading while the rainband was stationary

Another case of downdraft modification of the boundary layer was observed during the lower three passes (at 270, 140, and 80 m altitudes) of the first stepped-descent profile on the inner side of the band from 1923 to 1927 UTC. At this time the rainband was stationary and exhibited a spiral horizontal reflectivity structure. The lower two levels of the profile intersected a gust front (discussed in Part I), which is evident as 15–20 m s^{-1} winds at the 80 m level in the horizontal TA radar reflectivity plot of Fig. 10. The aircraft was in a no-cloud region between the primary rainband to the right and a secondary rainband (stratiform precipitation) to the left. Dewpoint depressions for this part of the profile ranged from 2–5 K and a rain "curtain" could be observed on each side of the aircraft through much of the pattern. At the end of the 80 m leg the aircraft was forced to ascend due to a heavy rain shower falling from the anvil at 1932 UTC.

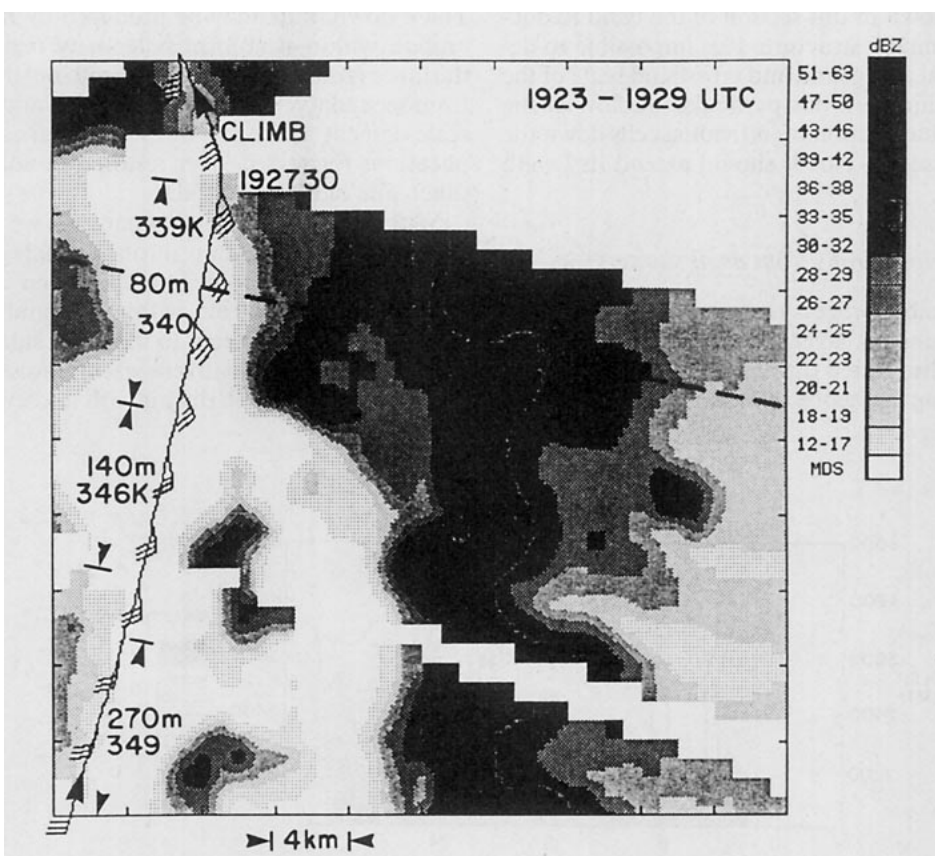

FIG. 10. Stepped-descent flight track adjacent to the Earl rainband displayed on a 40 × 40 km TA radar composite (inset box in Fig. 8b). Numbers on track refer to altitude in m and equivalent potential temperature (θ_E) in K. Dashed line indicates location of Doppler cross section shown in Fig. 11.

(Sounding 20 in Fig. 4a was taken during this climb.)

As shown by the θ_E values plotted adjacent to the flight track in Fig. 10, the aircraft passed through successively lower θ_E air while descending from 270 to 80 m over a distance of 30 km, with the lowest θ_E air (338 K) observed at 1926:50 UTC. A vertical cross section of reflectivity together with airborne Doppler radar observations of the wind component toward the radar (essentially the crossband component) at 1926:50 UTC (corresponding to the dashed line in Fig. 10) is presented in Fig. 11. The crossband wind component towards the aircraft suggested by the low-level Doppler measurements begins to increase from 5 m s^{-1} at the inner edge of the 35 dBZ echo to 11 m s^{-1} at 2 km from the aircraft.

Plots of the Doppler-measured wind (horizontal portion of the wind component in the direction of the beam) at several levels over the 40 × 40 km domain of Fig. 11 show that depth of the downdraft outflow is <1 km, with maximum speed at the lowest level (200 m), and a horizontal scale of at least 10 km (alongband) × 25 km (crossband). The lowest θ_E air sampled at this level had a trajectory from a section of the rainband where reflectivity cells reached as high as 45 dBZ. Unfortunately, no crossband passes or Doppler "L" patterns were flown in this section of the band to document the kinematic structure. It is impossible to determine the total alongband and crossband scale of the low θ_E air contained in this particular outflow of the Earl rainband, but motion of individual cells down the band, as discussed in Part I, should extend its length along the band.

c. *Penetrative downdrafts from anvil showers*

Another possible process contributing to modification of the boundary layer on the inner side of the rainband was discovered during the climb from 80 to 1500 m following the stepped-descent profile. Sounding 20 in Fig. 4a was made in a heavy (1–2 mm h^{-1}) rain shower from the anvil overhanging the inner side of the band. Although no accurate vertical motions were available during the climb, the last 10 s of w measurements at the 80 m level indicate downward motion of up to −1.5 m s^{-1}. Sounding 20, (Fig. 4a) which began just after 1926:54 UTC, indicates two layers of air, each concerned with a specific process that can modify the boundary layer. The lower layer, from the bottom (80 m) to 960 mb (~400 m), is very stable and represents the low (339–340 K) θ_E air spreading outward from the band axis as a gust front (discussed above). The layer above 960 mb represents an unsaturated downdraft of 342 K θ_E air associated with rain falling from the stratiform reflectivity region on the inner side of the band. This air is warming and drying during descent, reaching a dewpoint depression of 5 K before detraining and mixing with the lower θ_E air spreading from the rainband. Near the end of the climb at an altitude of 1135 m, liquid water measurements indicated that the aircraft was passing through both cloud and rain.

The observations suggest that mesoscale descent and occasional convective-scale penetrative downdrafts are present on the inner side of outer convective rainbands. These downdrafts may be produced by rainfall evaporation within stratiform reflectivity regions beneath the inner rainband anvil and beneath outer anvil clouds from secondary rainbands. Mesoscale and convective-scale descent at the top of the HPBL has serious implications for mixed-layer restoration adjacent to the inner side of the rainband.

With these additional mechanisms we can hypothesize a sequence of events through which growth of the mixed layer is severely limited. When a convective downdraft outflow from within the rainband spreads out at low levels adjacent to the inner side of the band (Figs. 10, 11), the relatively warm, moist, lower level air is replaced by cool, dry air with midlevel properties

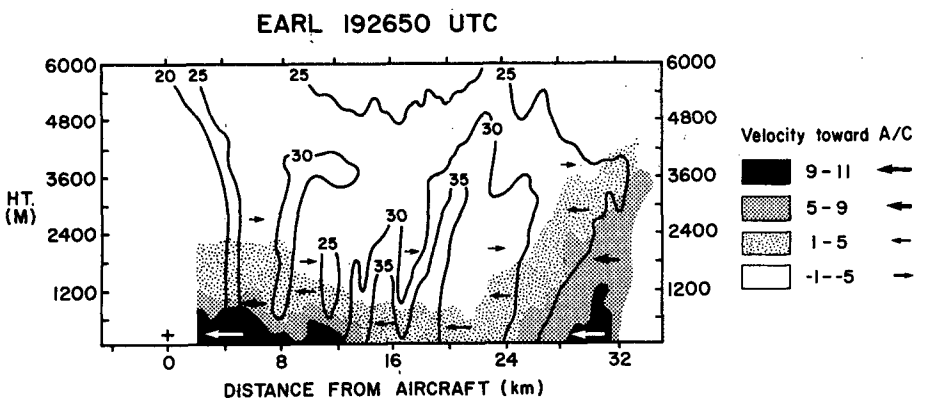

FIG. 11. Cross section of Doppler radar measured wind component in the direction of the beam over one sweep showing downdraft outflow accelerating from band axis (~15 km from aircraft). Cross section is to right of track along dashed line in Fig. 10.

(low θ_E) and the mixed layer is destroyed. The air immediately begins to recover due to surface fluxes of heat and moisture and turbulent entrainment of high Θ air from above. This restoration process is then hindered, or even halted temporarily, when additional downdrafts, originating in the stratiform anvil rain adjacent to the inner side of the band detrain at the top of the shallow, developing mixed layer (as implied by sounding 20 in Fig. 4a). Even without additional downdrafts, the recovery process may be slowed by mesoscale subsidence atop the HPBL which frequently occurs between eyewall convection and the first outer rainband, producing the characteristic "moat region" in visible satellite imagery. Entrainment of warm dry air overlying the HPBL in this region will aid in restoration of dry static energy but will hinder water vapor recovery within the mixed layer.

5. Recovery of the disturbed mixed layer

If we consider that well-organized outer convective hurricane rainbands have length scales of ~200 km or more and that the inner side of these bands is occupied by a region of low moist static energy (H) throughout the band lifecycle (as suggested by Fig. 8b), we can envision recovery of such air along a trajectory while mixing horizontally and vertically under increasing wind speeds in a region of mesoscale low-level convergence and upward surface heat and moisture fluxes. However, these restorative processes may be counteracted by the quantity of low H air, mesoscale between-band divergence above the boundary layer, and the evaporation of stratiform rain falling from the eyewall and secondary rainband anvils, which cools but also moistens the mixed layer.

In this section, boundary layer recovery is explored through mixed-layer model calculations made along flow trajectories from the inner sides of rainbands in Hurricanes Earl and Floyd towards their eyewalls. The model is described briefly, its application to the hurricane is examined, and its results and sensitivity to initial conditions and specified parameters is investigated.

a. Mixed-layer recovery model

Simple mixed-layer jump models have been used by Zipser (1977) and Fitzgarrald and Garstang (1981b) to study the recovery and maintenance of the mixed layer in tropical squall-line wakes. These models are highly idealized versions of a model first developed by Lilly (1968) and assume that a convective (in the sense that buoyancy-generated turbulence prevails) mixed layer of depth h is capped by an infinitesimally thick stable transition layer above which the atmospheric lapse rates of dry static energy (Γ_S) and specific humidity (Γ_q) are specified as depicted in Figs. 5b and 6b. In their study of the boundary-layer recovery within a tropical squall-line wake, Nicholls and Johnson (1984) presented results from the "General Structure Entrainment Model" (GSEM) developed by Deardorff (1979), which included transition layer physics. Nicholls and Johnson found that the GSEM was well suited to including the diabatic heating and moistening effects of precipitation evaporation in the mixed and transition layers, which were not taken into account in the model calculations of Zipser (1977) and Fitzgarrald and Garstang (1981b). The reader is referred to the appendix of Nicholls and Johnson's paper, Deardorff (1979), and Powell (1988) for further details on the model and a development of the GSEM equations.

As discussed by Nicholls and Johnson (1984), the GSEM involves equations for mixed layer growth, dry virtual static energy (s_V), specific humidity (q), vertical flux of q, and entrainment velocity (W_E) all at the top of the mixed layer (h). The thickness of the transition layer (Δh), and jumps of s_V(Δs_V) and q(Δq) between h and the top of the transition layer (as depicted for sounding 11 in Figs. 5b, 6b) are also evaluated.

Surface fluxes of sensible heat (F_S) and moisture are calculated by the bulk aerodynamic method employing the neutral stability turbulent heat and moisture exchange coefficients according to Large and Pond (1982). This method has obvious drawbacks since the observations necessary to determine proper transfer coefficients are very difficult to make and have never been made in the extreme conditions characteristic of hurricanes. The Large and Pond transfer coefficients are the best available at this writing. These coefficients depend on the surface wind speed and were based upon a large set of direct flux measurements in the highest wind speed conditions available (up to 25 m s^{-1} for sensible heat and 15 m s^{-1} for latent heat flux). Sea spray contributions to the latent heat flux (Powell 1988) may be important but are not included in the flux calculation. Sea surface virtual potential temperatures and specific humidity were determined by assuming saturation values at the observed sea surface temperature.

According to Deardorff (1979), the GSEM is applicable, provided buoyancy-driven entrainment exceeds shear-driven entrainment such that ($\Delta V/6W_*$) < 1. Here ΔV is the jump in the mean wind speed across the transition layer and W_* is the convective scale velocity defined as

$$W_* = [ghF_S/\rho s_V]^{1/3} \quad (1)$$

where g is the gravitational constant and ρ is air density. Calculations of ($\Delta V/6W_*$) for a hurricane mixed layer that is adjacent to the Earl rainband range between 0.4 and 0.8 and are similar to values calculated by Nicholls and Johnson (1984), suggesting that GSEM usage may be appropriate for outer hurricane rainband areas.

b. Application of the GSEM to the hurricane mixed layer

Mixed-layer restoration calculations were made along the trajectories adjacent to the outer rainbands in Earl (Fig. 12a) and Floyd (Fig. 12b). These trajectories are representative of storm-relative, mean mixed layer flow and were determined (for Earl) by using the 150 m level inflow angle and 90% of the 1500 m level winds from an earlier survey pattern. It is assumed that the storm-relative flow field is in steady state and that structure and intensity do not change during the time period of the trajectory. Trajectories in Floyd were determined based on the 150 m level winds on the inner side of the band as shown in the schematic of BZJM.

Based upon observations of cloud base in the area of interest on the inner side of the band, and on the condition that the recovery inflow occurs in a suppressed region between the eyewall and the outer rainband, the mixed layer is assumed to be well below cloud base (500–700 m) at all times. The diabatic heat and moisture contributions of rainfall evaporation are computed as described by Nicholls and Johnson (1984), using a precipitation drop-size spectrum parameter (their lambda = 80 cm^{-1}) appropriate for the drop size distributions presented by Willis (1984). Rainfall rates were determined by applying the hurricane reflectivity-rainfall rate (Z–R) relationship (Jorgensen and Willis 1982) to composite radar reflectivity observations along the inflow trajectory. Rainfall rates

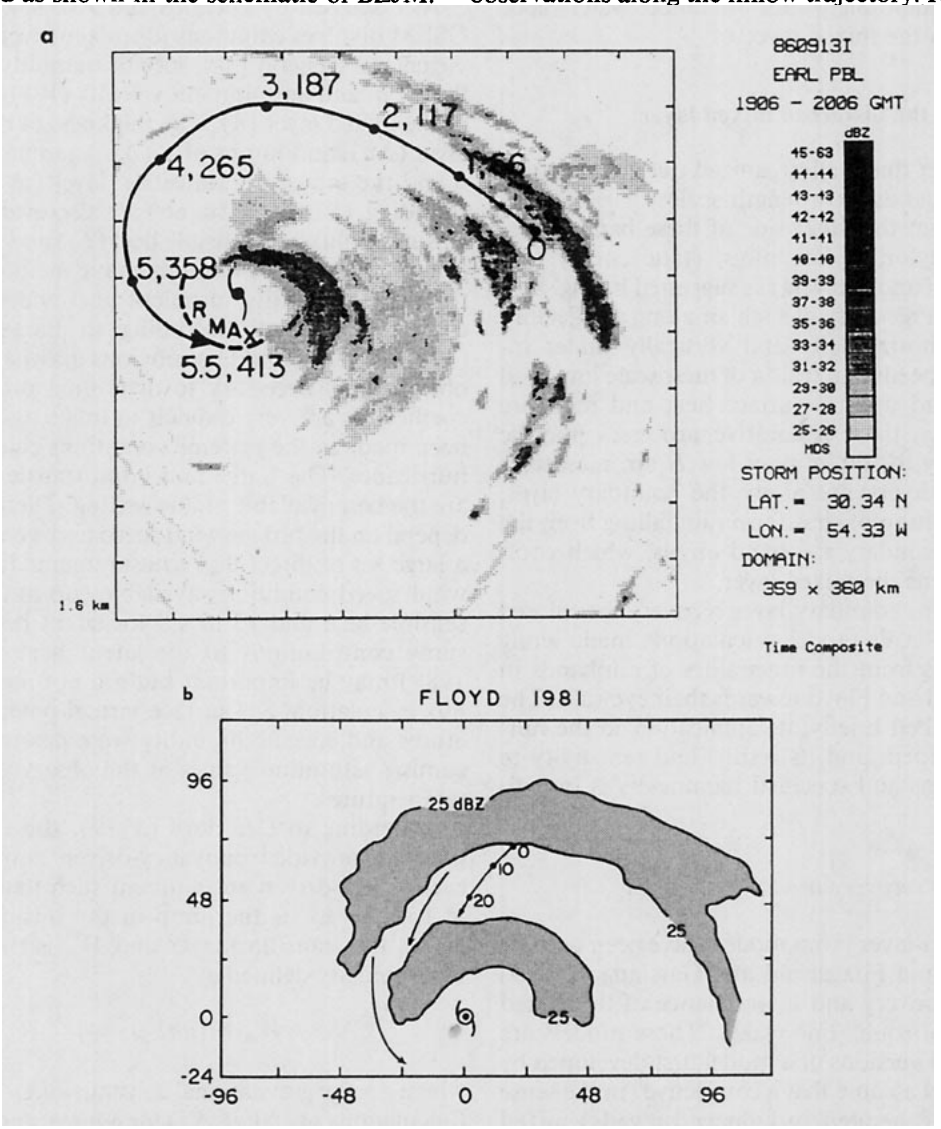

FIG. 12. Mean mixed layer trajectories from a downdraft-modified boundary layer region on the inner side of rainbands: (a) in Hurricane Earl over a 360 × 360 km LF radar reflectivity composite, numbers refer to elapsed time (h) and distance (km) along trajectory, (b) in Hurricane Floyd over a 216 × 144 km radar reflectivity schematic, numbers along trajectory refer to time (min) from initial point.

varied between 0.4 and 1.2 mm h^{-1} for the Earl trajectory and between 0.6 and 1.2 mm h^{-1} for the Floyd trajectory, well below the 2 mm threshold determined to be associated with penetrative downdrafts (Barnes and Garstang 1982). Surface fluxes of heat and moisture are allowed to interact with the recovery by computation at each time step.

Initial quantities for mixed-layer depth (h_1), transition layer top (h_2), θ_E, s, Δs, γ_S, γ_q, q, and Δq were taken from soundings 19, and a combination of 11 and 20 (Figs. 5 and 6) representative of the disturbed conditions on the inner side of the Earl rainband. Sounding 11 was adjusted to have the same surface s, q, and H values as were found in sounding 20, the most disturbed sounding, and is thus labeled sounding 11A. Two types of soundings with negative (sounding 19) and positive (sounding 11A) specific humidity jumps at the transition layer, were used for each model run since disturbed soundings exhibited both types of profiles. A constant value of 27°C was chosen for the SST along the trajectory based upon airborne radiometer, Air-Expendable Bathythermographs (AXBTs) and post-storm satellite observations.

Vertical motion values for the top of the mixed and transition layer were specified by assuming constant divergence (div) at the top of the mixed and transition layers ($w = -h \cdot \text{div}$). The initial value of div (10^{-4} s^{-1}) was calculated from 1500 m level data (from the Earl survey pattern) closest to the trajectory and is considered to be representative of downward mesoscale motion that occurs in suppressed regions between the eyewall and outer rainband. As the eyewall is approached, at the 350 km, 4.6 h point in Fig. 12 (and the 26 km, 16 min point for Floyd), the divergence is changed to negative to represent mesoscale upward motion.

Trajectory quantities of rainfall rate and surface pressure were determined from lower fuselage radar observations, and 1500 m level survey pattern pressure measurements extrapolated hydrostatically to the surface. Earth-relative surface (10 m) windspeed values required for surface flux calculations were estimated through use of a diagnostic marine boundary layer model (Powell 1980, 1987). The above quantities were interpolated along the trajectory by a standard cubic spline routine at a 1 km interval. The GSEM equations were integrated forward in space at a 1 km spatial step along the trajectory, using forward centered differencing (as suggested by Melville Nicholls, Colorado State University, personal communication, 1988).

c. *Calculations of hurricane mixed-layer recovery*

Results for the GSEM computations of h, θ_E, s and q for both Earl and Floyd trajectories are presented in Figs. 13a–d. Initial data for the calculations in Earl and Floyd are listed in Table 2. The initial disturbed mixed layer depth (h_1), is 100 m for all runs while the top of the transition layer (h_2) is 200 m for sounding 11a and 350 m for sounding 19. Note that trajectory lengths for Earl are a factor of 10 longer than for Floyd. For both Earl cases the mixed-layer depth, h in Fig. 13a, recovered to near normal (400–500 m) heights by 200 km. The θ_E recovery, however, (Fig. 13b) is only near complete for sounding E19, while Ella never recovers to a value close to that which had been observed in undisturbed soundings on either side of the rainband (Fig. 8a). The main difference between the two runs is in the initial specific humidity jump, Δq, for the transition layer. Run E11A starts with a negative jump, decrease of q of 1 g kg^{-1} from h_1 to h_2, while E19 begins with a positive jump of 2.5 g kg^{-1}. Throughout the trajectory, s (Fig. 14c) increases slowly but steadily, due to downward mixing (entrainment) of high s air from above and surface sensible heat fluxes. The changes in q (Fig. 13d) parallel those of θ_E such that q may actually decrease along the trajectory. Nicholls and Johnson (1984) and Fitzgarrald and Garstang (1981b) attributed this result to the entrainment of relatively dry air from above the mixed layer that exceeded the enrichment of moist air due to surface fluxes and rainfall evaporation. The model calculations suggest that this drying is very dependent on the jump of specific humidity across the transition layer.

Results of the GSEM for Hurricane Floyd show that the trajectory is too short for the mixed-layer depth to recover past 300 m before reaching the vicinity of the eyewall. The run for sounding F19 achieved θ_E recovery before reaching the eyewall, but F11a could not recover past 347 K (BZJM indicate undisturbed θ_E values of 350–354 K on the outer side of the Floyd rainband).

d. *Sensitivity of restoration to initial and specified conditions*

Numerous GSEM runs were made to investigate the sensitivity of the mixed layer restoration calculations to changes in some of the initial conditions and specified parameters. Results of the model sensitivity for Hurricanes Earl and Floyd are listed in Tables 3 and 4. The control runs for sensitivity tests of both storms were as given in Table 2, and were discussed above. The most important factors affecting model calculations of mixed layer recovery included: divergence magnitude, rainfall rate, Γ_q, Δq, SST, and w. For comparison purposes, the runs for sounding 19 (E19 and F19 discussed above) were also included in Tables 3 and 4.

Divergence. For the Earl calculations, an increase of divergence by a factor of 5 drastically cut down on mixed-layer deepening. Entrainment was sufficient to dry the mixed layer, but not large enough to allow h to increase against a strong downward vertical velocity at the top of the mixed layer.

Rainfall. Increasing the rainfall rate from zero to the control acts to promote greater mixed-layer depth through increased entrainment, yet slower recovery of

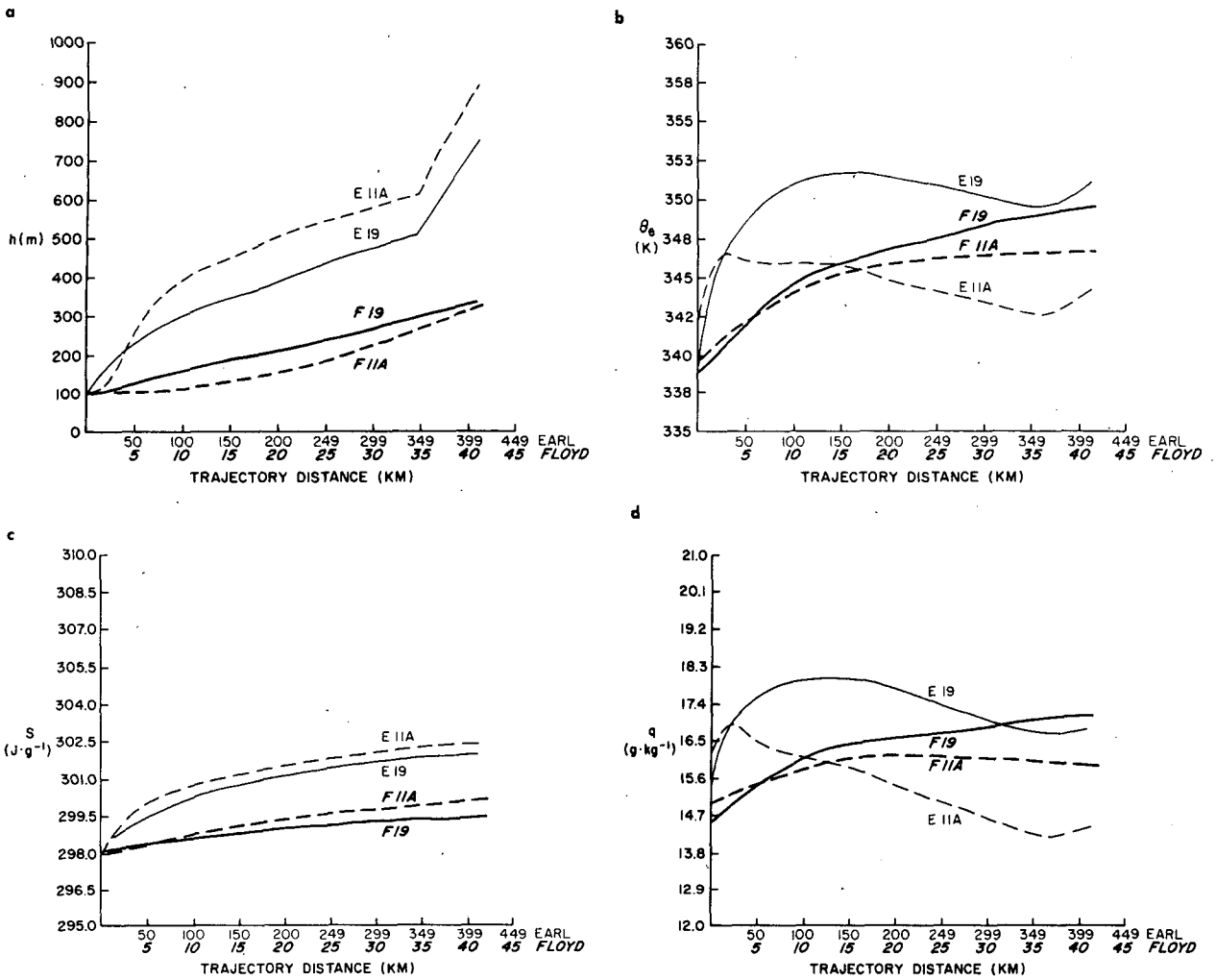

FIG. 13. General Structure Entrainment Model (GSEM) results for mixed layer development along trajectories in Hurricanes Earl (E) and Floyd (F) for initial condition soundings of Table 2. (a) Mixed layer depth (h), (b) equivalent potential temperature (θ_E), (c) dry static energy (S), (d) specific humidity (q).

θ_E through drying. The reason for this increased entrainment is the instability produced by differential evaporation as the rain falls through the transition layer. Evaporative cooling at the top of the transition layer (with smaller q) exceeds cooling at the bottom (larger q), resulting in enhanced turbulent mixing.

TABLE 2. Mixed-layer recovery model initial conditions.

Initial quantity	Earl (11A)	Earl (19)	Floyd (11A)	Floyd (19)
h_1 (m)	100.	100.	100.	100.
h_2 (m)	200.	350.	200.	350.
θ_E (K)	341.8	339.0	340.1	338.7
s (J g^{-1})	298.1	298.1	298.1	298.1
Δs	1.6	1.6	1.6	1.6
Γ_s (J kg^{-1} m^{-1})	4.1	4.1	4.1	4.1
q (g kg^{-1})	16.0	15.0	15.0	14.5
Δq	−1.0	+2.5	−1.0	+2.5
Γ_q (10^{-6} m^{-1})	−6.25	−6.25	−6.25	−6.25
div (10^{-4} s^{-1})	1.0	1.0	1.0	1.0
SST (K)	27.	27.	27.	27.

Specific humidity profile. A -1×10^{-6} m^{-1} increase of Γ_q allows Δq to become larger, thereby enhancing the rainfall evaporation effects and mixing drier air into the mixed layer. Doubling Δq displays the same effect.

Sea surface temperature. A 1°C reduction in SST slows mixed-layer growth and entrainment drying by decreasing surface sensible heat and moisture fluxes, which causes a larger Δs_V and smaller Δq than the control (more stability) resulting in a lower entrainment velocity. With weaker entrainment however, less dry air is mixed into the mixed layer and θ_E is slightly higher than the control upon reaching the eyewall vicinity. The effect of cooler water on surface fluxes will hinder mixed layer redevelopment (maintenance) most

TABLE 3. Mixed-layer model recovery sensitivity (Earl).

Sensitivity parameter	Time (h:min)/Distance on trajectory (km)							
	0:44/50	1:45/100	2:30/150	3:17/200	3:41/250	4:10/300	4:39/350	5:20/400
Control E11A: h = 100	255.	390.	448.	505.	544.	580.	617.	840.
q^1 = 16	16.5	16.1	15.9	15.4	15.0	14.6	14.3	14.3
θ_E = 341.8	341.6	345.9	345.7	344.8	344.2	343.4	342.6	343.7
No rain	224.	336.	363.	362.	353.	342.	332.	446.
	16.7	16.4	16.4	16.5	16.6	16.8	17.0	17.2
	346.6	346.8	347.5	348.2	349.	350.	350.9	352.4
Divergence increase from 1 to 5 ($\times 10^{-4}$ s^{-1})	188.	193.	175.	165.	148.	139.	138.	458.
	15.6	14.6	13.8	13.2	13.0	12.9	12.9	13.6
	344.	342.3	340.9	339.6	339.6	339.6	340.	342.8
Γq increased from -6.25 to -7.25 ($\times 10^{-6}$ m^{-1})	264.	412.	480.	551.	603.	652.	704.	963.
	16.4	15.8	15.3	14.6	14.0	13.4	12.8	12.8
	345.7	344.9	344.2	342.6	341.3	339.9	338.5	339.2
Initial Δq increased from -1 to -2 (g kg^{-1})	271.	407.	466.	526.	567.	606.	647.	880.
	15.8	15.3	15.1	14.6	14.2	13.8	13.4	13.5
	344.	343.7	343.5	342.5	341.7	341.	340.2	341.2
SST reduced from 27° to 26°C	176.	296.	346.	394.	428.	459.	491.	667.
	16.8	16.5	16.3	16.0	15.7	15.4	15.1	15.3
	346.7	346.5	346.5	345.8	345.3	344.8	344.3	345.4
W = 0	286.	501.	641.	—	—	—	—	—
	16.7	16.5	16.6	—	—	—	—	—
	346.5	346.8	347.4	—	—	—	—	—
Sounding E19: h_1 = 100	232.	302.	346.	390.	437.	476.	514.	705.
q^1 = 15	17.5	17.9	17.9	17.7	17.3	17.0	16.7	16.7
θ_E = 339	348.6	351.0	351.7	351.5	351.0	350.3	349.7	350.7

TABLE 4. Mixed-layer model recovery sensitivity (Floyd).

Sensitivity parameter	Time (min:sec)/Distance along trajectory (km)						
	3:34/5	7:09/10	10:00/15	12:30/20	15:37/25	18:11/30	21:13/35
Control F11A: h = 100	108.	119.	135.	157.	185.	223.	266.
q^1 = 15	15.5	15.9	16.1	16.1	16.1	16.0	16.0
θ_E = 340.1	342.4	344.2	345.3	345.9	346.2	346.4	346.5
No rain	107.	118.	133.	154.	180.	215.	255.
	15.5	15.9	16.1	16.2	16.1	16.1	16.0
	342.4	344.2	345.3	345.9	346.3	346.5	346.7
Divergence increase from 1 to 5 ($\times 10^{-4}$ s^{-1})	100.	104.	114.	131.	156.	209.	276.
	15.5	15.9	16.1	16.1	16.0	15.8	15.7
	342.5	344.4	345.5	346.0	346.1	346.0	345.9
Γq increased from -6.25 to -7.25 ($\times 10^{-6}$ m^{-1})	107.5	119.	135.	157.	186.	226.	271.
	15.5	15.9	16.1	16.1	16.1	16.0	15.9
	342.4	344.2	345.3	345.9	346.1	346.2	346.2
Initial Δq increased from -1 to -2 (g kg^{-1})	108.	119.	136.	159.	188.	227.	272.
	15.4	15.7	15.8	15.8	15.7	15.5	15.4
	342.2	343.7	344.5	344.9	344.9	344.9	344.9
SST reduced from 27° to 26°C	105.	112.	120.	131.	144.	164.	190.
	15.4	15.8	16.0	16.2	16.3	16.3	16.3
	342.1	343.7	344.8	345.7	346.3	346.8	347.1
W = 0	110.	123.	142.	165.	195.	229.	266.
	15.5	15.9	16.1	16.1	16.1	16.1	16.0
	342.4	344.1	345.2	345.8	346.2	346.4	346.6
Sounding F19: h_1 = 100	128.	159.	187.	213.	238.	267.	299.
q^1 = 14.5	15.5	16.1	16.4	16.6	16.7	16.8	17.0
θ_E = 338.7	342.3	344.7	346.0	346.8	347.6	348.3	349.0

severely when a recovering (undisturbed) mixed layer encounters a cold SST wake area (Peter G. Black 1988, personal communication).

Vertical velocity. Without any downward vertical velocity to suppress it, when $W = 0$, the mixed layer grows rapidly over 150 km. A combination of weaker entrainment velocity at the mixed-layer top and negative entrainment velocities at the transition layer top (shrinking transition layer) forces Δs_V to zero by 175 km (at $h = 721$ m) and ends the calculation ($\Delta s_V < 0$ is not permitted).

The tests for the Floyd trajectory indicate mixed-layer sensitivity results that are similar to the Earl runs, although over a much shorter trajectory length. Runs with different Γ_q and Δq are similar to the control run, since these effects are only apparent for longer trajectories.

e. *Implications of incomplete recovery*

For realistic initial soundings that are characteristic of downdraft modification of the mixed layer and realistic specifications of suppressed conditions along inflow trajectories between the eyewall and principal rainband, it is apparent that some of the air reaching the eyewall may be deficient in moist static energy. This deficiency could decrease the depth of eyewall convection which could then feed back to decrease upper and middle-level heating. If θ_E is deficient over a large area adjacent to the eyewall, the core of the storm should be affected, resulting in a hydrostatic increase in the surface pressure and subsequent weakening of the storm.

It is important to emphasize that the GSEM does not include the contributions of shear-enhanced entrainment. Shear entrainment should increase W_E and the depth of the mixed layer, but this would also increase the mixing of dry air from above, further decreasing θ_E. Another physical mechanism not considered is the effect of turbulent lateral mixing along the trajectory. The edges of a region of downdraft air should mix considerably by this mechanism, depending upon the scale of the disturbed region. The effect of disturbed boundary-layer air on storm intensity and strength can only be resolved by additional measurements that are designed to determine the time scale of recovery and the spatial scale of modified regions of the rainband. As seen in the sensitivity study, the boundary layer recovery is very dependent on the humidity profile across the transition layer and above. Measurements of this quantity in the region between outer rainbands and the eyewall are very sparse, and must be collected in order to verify these calculations. Of equal necessity are mesoscale numerical model studies of the response of convection to a partially recovered mixed layer.

6. Summary and conclusions

High resolution boundary-layer experiments were conducted in quasi-stationary principal rainbands 230 km from the centers of Hurricanes Josephine (1984) and Earl (1986). The two rainbands contained many common features which are summarized in a schematic model of the two-dimensional mesoscale thermodynamic structure of an outer convective rainband in Fig. 14. This model is a companion to the model of the precipitation and kinematic structure described in Fig. 16b of Part I.

HPBL inflow toward the rainband axis from the outer side is characterized by a deep (500 m) mixed layer, which is modulated by subsidence and mesoscale downdrafts descending from precipitation falling from the outer anvil. The deep outer mixed layer contains air approaching the band that has had a long fetch over warm water without convective modification. If the band is convectively active, much of this air is entrained or forced into the convection within the band, mixing with vertical drafts as proposed by BZJM, while the rest may continue across the band, flowing around cells and through breaks in the band, as suggested by Zipser (1977). The high θ_E air that feeds the most intense cells is forced to rise just on the inner side of the band axis, either by a part of a cool spreading downdraft or by a barrier effect produced by strong convergence and mesoscale pressure forces generated by the band and contributes considerable convective available potential energy (CAPE) to the rainband. The air that reaches the inner side through breaks in the band maintains an undisturbed character, e.g., ODW soundings 1 and 10 in Fig. 5b.

Adjacent to intense reflectivity cells, the HPBL structure on the inner side of the rainband is dominated by spreading downdrafts carrying low θ_E air from middle levels ($\approx$850–700 mb). Outflow from an individual downdraft may extend 25 km or more from its parent reflectivity cell. An accumulation of cool dry air from convective scale downdrafts may be found on the inner side of the band axis occupying the boundary layer on alongband scales that are roughly the length of the convectively active portion of the rainband. The cross-band scale of modification in this region is at least 25 km and the actual extent awaits documentation in future experiments. If the downdrafts are sufficiently intense to reach the surface, the mixed layer may be completely destroyed. Disturbed air then begins recovery adjacent to the band along a trajectory over warm water and beneath precipitating anvil clouds. Along this trajectory the developing mixed layer may be subjected to further modification (discussed in section 4) by downdrafts penetrating to the HPBL in rain falling from the inner portion of the anvil cloud.

As yet, the three-dimensional structure of the flow is not clear. Individual cells and larger reflectivity elements make up the band, but we do not know the positions or shapes of the convective scale and mesoscale updrafts and downdrafts within these features. Analysis of airborne Doppler radar data collected in Earl is in progress and should help to clarify the three-dimensional circulation of the airflow in rainbands.

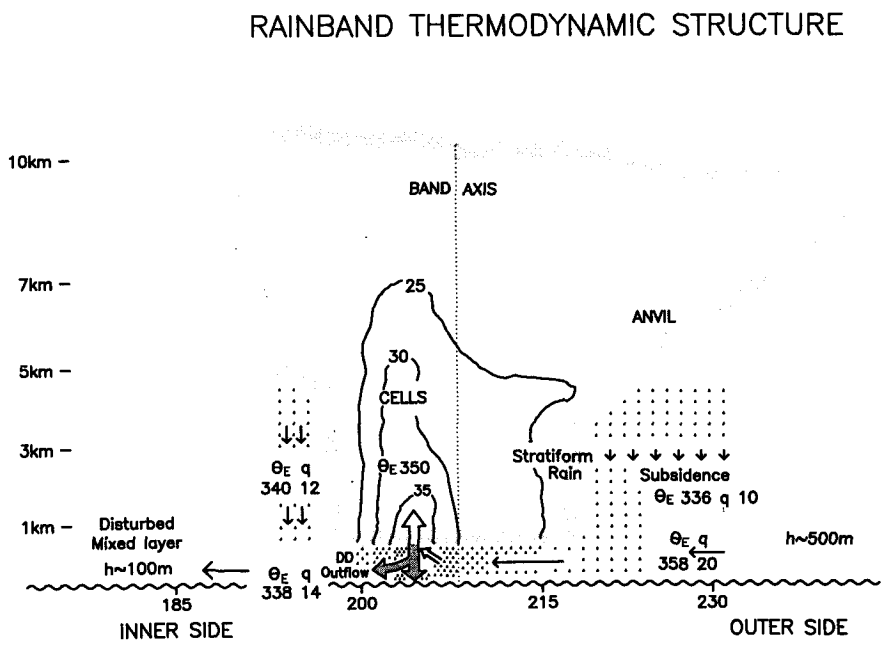

FIG. 14. Schematic cross section of the thermodynamic structure in the Hurricane Earl rainband. Outer solid contour indicates band cloud edges while other contours represent radar reflectivity. Horizontal arrows represent crossband component of the wind, bold vertical arrows indicate convective core updrafts and downdrafts, small downward arrows indicate mesoscale subsidence regions and larger downward arrows indicate penetrative downdrafts originating in the inner anvil region.

Mixed-layer model calculations were made to estimate the extent to which initially disturbed boundary-layer s and q profiles were restored to values characteristic of undisturbed conditions. The Nicholls and Johnson (1984) adaptation of the Deardorff (1979), General Structure Entrainment Model (GSEM) was applied to trajectories initiated at the disturbed mixed-layer regions on the inner sides of the Earl and Floyd rainbands and ended at the respective outer portions of the eyewall. The calculations were made for initial conditions based upon observed aircraft and ODW soundings and assumed suppressed conditions (no clouds below the top of the transition layer) between the outer rainband and the eyewall. Restoration of the hurricane mixed layer depends on the supply of heat and moisture to the mixed layer by fluxes from the surface and by fluxes across the top of the mixed layer (entrainment). Entrainment is most sensitive to rainfall evaporation, divergence at the top of the mixed and transition layers, the lapse rate (above) and jump (within) of specific humidity within the transition layer, and the SST distribution along the inflow trajectory.

As found in the model calculations of tropical squall-line wake recovery by Nicholls and Johnson (1984), the moistening effect of rain evaporation (from anvil precipitation) is overcome by an increase in entrainment produced by differential evaporation cooling over the transition layer. This entrainment mixes down drier air from above, reducing the recovery of θ_E despite growth of the mixed layer to predisturbed heights of 500 m. For the Earl band, a maximum recovery (defined as the ratio of model-calculated θ_E increase to that required (10K) to restore θ_E to undisturbed (352 K) conditions) of 40% occurred in the first 50 km, after which entrainment drying reduced recovery to near zero by 350 km. For much shorter trajectories in Floyd, recovery occurred throughout the trajectory, but only reached 55%–70% of that required for complete θ_E restoration upon reaching the eyewall.

Incomplete mixed-layer recovery implies that the low-level θ_E air entering the eyewall convection will release less CAPE leading to shallower convection, less latent- and compensating subsident heating at middle and upper levels, and a corresponding hydrostatic pressure rise in the eye. Hence, modification of the boundary layer by rainband downdrafts may be responsible for changes in the storm intensity.

At present, we do not know enough about the spatial and temporal scales of the disturbed mixed layer or the degree to which incompletely recovered air reaches the eyewall to verify these model calculations. The model results point to HPBL modification as a possible mechanism for transitional changes in hurricane intensity and strength. Much additional work is required to determine appropriate entrainment mechanisms in strong winds over water. Improvements and development of turbulence instrumentation on the NOAA hurricane research aircraft have the potential to obtain the data required to answer many remaining questions on the turbulent kinetic energy budget and structure

within the HPBL. This is a promising area for future research.

Acknowledgments. The author benefitted from many helpful discussions with Peter Black and Paul Willis of the NOAA Hurricane Research Division (HRD), and with Gary Barnes of NCAR. Mel Nicholls and Dick Johnson of Colorado State University graciously supplied the code and advice for the GSEM calculations. Much of the software for airborne Doppler radar analysis was developed by Frank Marks of HRD. Neal Dorst and Joyce Berkeley provided valuable software development and data processing assistance. The author is grateful for the support of Stanley Rosenthal and Bob Burpee of HRD and T. N. Krishnamurti, Noel LaSeur, Raymond Staley, Steve Stage, and Peter Black of his Ph.D. committee at The Florida State University.

REFERENCES

Anthes, R. A., and S. W. Chang, 1978: Response of the hurricane boundary layer to changes in sea surface temperature in a numerical model. *J. Atmos. Sci.*, **35**, 1240–1255.

Barnes, G. M., and M. Garstang, 1982: Subcloud layer energetics of precipitating convection. *Mon. Wea. Rev.*, **110**, 102–117.

——, and G. J. Stossmeister, 1986: The structure and decay of a rainband in Hurricane Irene (1981). *Mon. Wea. Rev.*, **114**, 2590–2601.

——, E. J. Zipser, D. P. Jorgensen and F. D. Marks, Jr., 1983: Mesoscale and convective structure of a hurricane rainband. *J. Atmos. Sci.*, **40**, 2125–2137.

Betts, A. K., 1976: The thermodynamic transformation of the tropical subcloud layer by precipitation and downdrafts. *J. Atmos. Sci.*, **33**, 1008–1020.

——, and J. Simpson, 1987: Thermodynamic budget diagrams for the hurricane subcloud layer. *J. Atmos. Sci.*, **44**, 842–849.

Black, P. G., 1983: Ocean temperature changes induced by tropical cyclones. Ph.D. dissertation, The Pennsylvania State University, 278 pp. [UMI 300 N. Zeeb Rd., Ann Arbor, MI, 48106.]

——, R. L. Elsberry, L. K. Shay, R. P. Partridge and J. F. Hawkins, 1988: Atmospheric and oceanic mixed-layer observations in Hurricane Josephine obtained from air-deployed drifting buoys and research aircraft. *J. Atmos. Oceanic Technol.*, **5**, 683–698.

Brown, J. M., 1979: Mesoscale unsaturated downdrafts driven by rainfall evaporation: A numerical study. *J. Atmos. Sci.*, **36**, 313–338.

Burpee, R. W., D. G. Marks and R. T. Merill, 1984: An assessment of Omega dropwindsonde data in track forecasts of Hurricane Debby (1982). *Bull. Amer. Meteor. Soc.*, **65**, 1050–1058.

Byers, H. R., 1944: *General Meteorology*. McGraw Hill, 645 p.

Deardorff, J. W., 1979: Prediction of convective mixed-layer entrainment for realistic capping inversion structure. *J. Atmos. Sci.*, **36**, 424–436.

Emanuel, K. A., 1986: An air–sea interaction theory for tropical cyclones. Part I: Steady state maintenance. *J. Atmos. Sci.*, **43**, 585–604.

——, 1988: The maximum intensity of hurricanes. *J. Atmos. Sci.*, **45**, 1144–1155.

Fitzgarrald, D. R., and M. Garstang, 1981a: Vertical structure of the tropical boundary layer. *Mon. Wea. Rev.*, **109**, 1512–1526.

——, and ——, 1981b: Boundary-layer growth over the tropical ocean. *Mon. Wea. Rev.*, **109**, 1762–1772.

Frank, W. M., 1977: The structure and energetics of the tropical cyclone II: Dynamics and energetics. *Mon. Wea. Rev.*, **105**, 1136–1150.

Franklin, J. L., S. J. Lord and F. D. Marks, Jr., 1988: Dropwindsonde and radar observations of the eye of Hurricane Gloria (1985). *Mon. Wea. Rev.*, **116**, 1237–1244.

Gamache, J. F., and R. A. Houze, Jr., 1982: Mesoscale air motions associated with a tropical squall line. *Mon. Wea. Rev.*, **110**, 118–135.

Johnson, R. H., and M. E. Nicholls, 1983: A composite analysis of the boundary layer accompanying a tropical squall line. *Mon. Wea. Rev.*, **111**, 308–319.

Jorgensen, D. P., and P. T. Willis, 1982: A Z–R relationship for hurricanes. *J. Appl. Meteor.*, **21**, 356–366.

Large, W. G., and S. Pond, 1982: Sensible and latent heat flux measurements over the ocean. *J. Phys. Oceanogr.*, **12**, 464–482.

Leary, C. A., 1980: Temperature and humidity in mesoscale downdrafts. *J. Atmos. Sci.*, **37**, 1005–1012.

LeMone, M. A., 1980: On the difficulty of measuring temperature and humidity in cloud: Comments on "Shallow convection on day 261 of GATE: Mesoscale arcs." *Mon. Wea. Rev.*, **108**,1702–1705.

——, 1983: Momentum transport by a line of cumulonimbus. *J. Atmos. Sci.*, **40**, 1815–1834.

Lilly, D. K., 1968: Models of cloud-topped mixed layers under a strong inversion. *Quart. J. Roy. Meteor. Soc.*, **94**, 292–309.

Lord, S. J., H. E. Willoughby and J. M. Piotrowicz, 1984: Role of a parameterized ice-phase microphysics in an axisymmetric, nonhydrostatic tropical cyclone model. *J. Atmos. Sci.*, **41**, 2836–2848.

Malkus, J. S., and H. Riehl, 1960: On the dynamics and energy transformations in steady-state hurricanes. *Tellus*, **12**, 1–20.

Merceret, F. J., and H. W. Davis, 1981: The determination of navigational and meteorological variables measured by NOAA/RFC WP3D aircraft. NOAA Tech. Memo., ERL RFC-7, AOML, 4301 Rickenbacker Cswy., Miami, FL 33149, 21 p.

Moss, M. S., 1978: Low-level features of two limited-area hurricane regimes. NOAA Tech. Rep. ERL 394-NHEML1. AOML/HRD Miami, FL 33149, 47 pp.

Merrill, R. T., 1988: Environmental influences on hurricane intensity. *J. Atmos. Sci.*, **45**, 1678–1687.

Nicholls, M. E., and R. H. Johnson, 1984: A model of tropical squall line boundary layer wake. *J. Atmos. Sci.*, **41**, 2774–2792.

Ooyama, K., 1969: Numerical simulation of the life-cycle of tropical cyclones. *J. Atmos. Sci.*, **26**, 3–40.

Powell, M. D., 1980: Evaluations of diagnostic marine boundary layer models applied to hurricanes. *Mon. Wea. Rev.*, **108**, 757–766.

——, 1987: Changes in the low-level kinematic and thermodynamic structure of Hurricane Alicia (1983) at landfall. *Mon. Wea. Rev.*, **115**, 75–99.

——, 1988: Boundary layer structure and dynamics in outer hurricane rainbands. Ph.D. Dissertation, Department of Meteorology, The Florida State University, 227 p., #8822464, UMI 300 N. Zeeb Rd., Ann Arbor, MI, 48106.

——, 1989: Boundary layer structure and dynamics in outer hurricane rainbands. Part I: Mesoscale rainfall and kinematic structure. *Mon. Wea. Rev.*, **117**, 891–917.

Rotunno, R., and K. A. Emanuel, 1987: An air–sea interaction theory for tropical cyclones. Part II: Evolutionary study using a nonhydrostatic axisymmetric numerical model. *J. Atmos. Sci.*, **44**, 542–561.

Rosenthal, S. L., 1978: Numerical simulation of tropical cyclone development with latent heat release by resolvable scales. I: Model description and preliminary results. *J. Atmos. Sci.*, **35**, 258–271.

Willis, P. T., 1984: Functional fits to some observed drop size distribution and parameterization of rain. *J. Atmos. Sci.*, **41**, 1648–1661.

Yamasaki, M., 1986: A three-dimensional tropical cyclone model with parameterized cumulus convection. *Papers in Meteor. Geophys.*, **37**, 205–234.

Zipser, E. J., 1969: The role of organized unsaturated convective downdrafts in the structure and rapid decay of equatorial disturbance. *J. Appl. Meteor.*, **8**, 799–814.

——, 1977: Mesoscale and convective-scale downdrafts as distinct components of squall-line circulation. *Mon. Wea. Rev.*, **105**, 1568–1589.